# A study of H I-selected galaxies in the Hercules cluster

Jorge Iglesias-Páramo, Willem van Driel, Pierre-Alain Duc, Polychronis Papaderos, Jose M. Vílchez, Véronique Cayatte, Chantal Balkowski, K. O'Neil, J. Dickey, H. Hernández, et al.

A&A 406, 453–469 (2003)
DOI: 10.1051/0004-6361:20030626


Astronomy & Astrophysics

# A study of H I-selected galaxies in the Hercules cluster⋆

J. Iglesias-Páramo[1], W. van Driel[2], P.-A. Duc[3], P. Papaderos[4], J. M. Vílchez[5], V. Cayatte[2], C. Balkowski[2], K. O'Neil[6], J. Dickey[7], H. Hernández[6], and T. X. Thuan[8]

[1] Laboratoire d'Astrophysique de Marseille, Traverse du Siphon – Les Trois Lucs, 13376 Marseille, France
e-mail: jorge.iglesias@oamp.fr
[2] Observatoire de Paris, GEPI, CNRS-UMR 8111 and Université Paris 7, 92195 Meudon Cedex, France
e-mail: wim.vandriel@obspm.fr; veronique.cayatte@obspm.fr; chantal.balkowski@obspm.fr
[3] CNRS URA 2052 and CEA, DSM, DAPNIA, Service d'Astrophysique, 91191 Gif-sur-Yvette Cedex, France
e-mail: paduc@cea.fr
[4] Universitäts-Sternwarte, Geismarlandstrasse 11, 37083 Göttingen, Germany
e-mail: papade@uni-sw.gwdg.de
[5] Instituto de Astrofísica de Andalucía (CSIC), Granada, Spain
e-mail: jvm@iaa.es
[6] Arecibo Observatory, HC3 Box 53995, Arecibo, Puerto Rico 00612, USA
e-mail: koneil@naic.edu, hhernand@naic.edu
[7] Department of Astronomy, University of Minnesota, 116 Church Street SE, Minneapolis, MN 55455, USA
e-mail: john@astro.umn.edu
[8] Astronomy Department, University of Virginia, Charlottesville, VA 22903, USA
e-mail: txt@astro.virginia.edu

Received 26 April 2002 / Accepted 9 April 2003

**Abstract.** The present study focuses on a sample of 22 galaxies detected in the blind VLA H I survey of the Hercules cluster by Dickey (1997), 18 of which were selected on an H I line width smaller than 270 km s$^{-1}$ and 4 others with only tentative optical counterparts in the Palomar Sky Survey. Sensitive single-dish H I line spectra were obtained for 20 of them, and for one the VLA detection was not confirmed. Optical surface photometry has been carried out for 10 objects, for 8 of which optical spectroscopy was obtained as well. Based on various criteria, we classify two sample galaxies (ce-143 and ne-204) as genuine dwarfs whereas the remaining sample objects are found to be intrinsically luminous galaxies. For those objects investigated in optical wavelengths we determine properties similar to those of actively star-forming galaxies, and find that approximately one half of them has properties intermediate between those of dwarf galaxies and low-luminosity disc galaxies. No optical redshifts could be determined for two of the galaxies (sw-103 and sw-194) and their physical association with the H I clouds detected at their positions therefore remains uncertain. A particularly interesting object in our sample is the Tidal Dwarf Galaxy candidate ce-061 in the galaxy merger IC 1182.

**Key words.** galaxies: abundances – galaxies: dwarf – galaxies: clusters: general – galaxies: clusters: individual: Hercules cluster

## 1. Introduction

It is well known from numerous studies based on observations and simulations that the environment plays a fundamental role in the evolution of bright galaxies, via galaxy-galaxy interactions and/or interactions of galaxies with the intergalactic medium. The present work is part of an ongoing study of the properties of H I-selected galaxies in clusters, for which the results on dwarfs in the Hydra cluster have already been published (Duc et al. 1999, 2001a; hereafter Papers I and II, respectively). The reasons for studying H I-selected objects are the sensitivity of H I to the environment and the selection of star-forming objects hosting H II regions, for which direct measurements of the metallicity are fairly easy. The most remarkable result is the existence of dwarfs with an oxygen abundance significantly higher than expected from the luminosity-metallicity relation for field dwarf galaxies.

In this paper we present single-dish 21 cm H I-line as well as optical imaging and spectroscopy observations of a sample of galaxies in the Hercules cluster, selected from the objects detected in the blind VLA H I line survey of the cluster by Dickey (1997). Our main aims are to study the structural

*Send offprint requests to*: J. Iglesias-Páramo,
e-mail: jorge.iglesias@oamp.fr

⋆ Appendix A and Figs. 5 to 12 are only available in electronic form at http://www.edpsciences.org

and spectrophotometric properties of these gas-rich galaxies, search for dwarfs among them and identify possible differences to the general galaxy population evolving within the cluster.

The Hercules supercluster is one of the most massive structures in the nearby Universe (Freudling 1995). It appears to be a collection of three clusters, gravitationally bound, but far from dynamical relaxation: Abell 2151, classified as richness class 2, and Abell 2147 and Abell 2152, both classified as richness class 1 (Barmby & Huchra 1998). In a previous single-dish study of the H I properties of a sample of galaxies in the Hercules supercluster, Giovanelli et al. (1981) found a strong deficiency in the H I mass-to-optical luminosity ratio of galaxies in the Abell 2147 cluster, while an almost normal, or mildly deficient, ratio was found for the galaxies in Abell 2151, the richest and densest of the three clusters. We have assumed a distance of 150 Mpc to the Hercules supercluster, based on an average redshift of 11 050 km s$^{-1}$ for the cluster spirals (see D97) and a Hubble constant of 75 km s$^{-1}$ Mpc$^{-1}$.

The paper is organized as follows: the sample selection and H I and optical observations are described in Sect. 2. The optical and H I properties of the sample galaxies are described in Sect. 3, and a discussion of the results is presented in Sect. 4. Comments on individual objects are given in the Appendix.

## 2. Observations

### 2.1. Sample selection

Our study of the Hercules cluster is aimed at H I-selected galaxies, as well as at reported H I clouds without optical counterparts on Digital Sky Survey (DSS) images, selected from the blind VLA 21 cm H I line survey of the cluster by Dickey (1997, hereafter D97) and reobserved by us at Arecibo in order to confirm the detections and to obtain H I line profiles with a better velocity resolution. Our failure to confirm the H I clouds without optical counterparts indicates that these were spurious, as described in van Driel et al. (2003).

In the first part of our project we have concentrated on H I-selected dwarf galaxies in the Hydra cluster (Papers I and II) from the VLA H I study by McMahon (1993), which has a velocity resolution of 42 km s$^{-1}$, similar to that of the D97 survey. We based on H I line widths at 20% of peak flux density value, $W_{20}$, smaller than 130 km s$^{-1}$, as objects with such narrow lines are good dwarf candidates. Of the 20 selected objects only 4 were found not to be dwarfs.

We could not apply such an effective H I line width criterion aimed at selecting dwarfs to the D97 data, however. As the Hercules cluster is about three times more distant (150 Mpc) than the Hydra cluster (45 Mpc), the H I profiles are correspondingly weaker and their widths more uncertain. The D97 H I mass detection limit of about $5 \times 10^8$ $M_\odot$ allows the detection of only the most gas-rich dwarf systems, while we estimate that the uncertainty in the FWHM line widths, $W_{50}$, is about 100 km s$^{-1}$ for the fainter H I detections, following Fouqué et al. (1990). We raised the cut-off value for $W_{50}$ to 270 km s$^{-1}$ for the Hercules cluster, thereby excluding only the most massive, inclined spiral systems.

All four fields of the D97 VLA study (three of which – ne, ce and sw – are located in Abell 2151, while the forth – 47 – is centred on Abell 2147) were covered in our Arecibo single-dish H I study. Of the total of 25 galaxies with optical counterparts in the Digital Sky Survey (DSS) and showing line widths smaller than 270 km s$^{-1}$ detected in the 4 fields by D97, we observed the following 18 in the H I line at Arecibo: ne-112, ne-142, ne-178, ne-204, ne-208, ne-240, ce-042, ce-048, ce-060, ce-061, ce-143, ce-176, ce-200, sw-103, sw-222, 47-138, 47-166 and 47-211. The 7 others were ruled out because they are very likely face-on spirals: ne-169, ne-222, ne-264, ce-122, ce-166, sw-159 and 47-030. In addition, we included in our list four galaxies showing line widths larger than 270 km s$^{-1}$ but with only tentative optical counterparts on the DSS (ne-250, ne-398, sw-194 and 47-154) in order to confirm the H I detections and to verify whether the optical associations are real or not. A summary of the observations obtained for our survey, together with the centre positions and $W_{50}$ line widths from D97, is given in Table 1.

For our optical imaging and spectroscopic observations, only the central (ce) and southern (sw) fields could be covered.

### 2.2. H I line observations

We made our H I line observations of the 22 H I-selected galaxies in the Hercules cluster with the refurbished 305 m Arecibo Gregorian radio telescope in May and June 2002. For further technical details on the observations and the data reduction we refer to van Driel et al. (2003).

The total net integration time (on+off) was on average 70 min per source, depending on the line strength, from 40 min for the strongest lines to 110 min for the weakest signals, in ne-398 and 47-154. The velocity coverage is about 2500 km s$^{-1}$, the velocity resolution is 1.3 km s$^{-1}$, and the telescope's half power beam width (HPBW) at 21 cm is $3\farcm4 \times 3\farcm6$. For the telescope's pointing positions the centre coordinates of the VLA H I sources as given in D97 were used (see Table 1 of D97). The data were reduced using IDL routines developed at Arecibo Observatory. A first-order baseline was then fitted to the data and the velocities were corrected to the heliocentric system, using the optical convention. All data were boxcar smoothed to a velocity resolution of 9.1 km s$^{-1}$ for further analysis, while the data of ne-398 and 47-154 were smoothed to 19.5 km s$^{-1}$.

### 2.3. Optical observations

Our optical observations are limited to objects in the ce and sw fields of the D97 survey. Of all 10 sample galaxies in these two fields we obtained deep CCD images, and low-to-medium resolution spectra for the 8 among these with the brightest optical counterparts (see Table 1).

#### 2.3.1. Optical imaging

*B*, *V* and *i*-band images were taken for most objects in our optical sample, except ce-143 and sw-222, for which only *V*

**Table 1.** Observations.

| Name | RA VLA (J2000.0) | Dec VLA | $W_{50}$ VLA (km s$^{-1}$) | H I det. Arecibo | Photom. | Optical emission lines |
|---|---|---|---|---|---|---|
| ne-112 | 16 06 37.6 | 18 23 49 | 262 | yes | | |
| ne-142 | 16 06 22.5 | 18 00 03 | 171 | yes | | |
| ne-178 | 16 06 13.8 | 17 57 11 | 217 | yes | | |
| ne-204 | 16 06 05.9 | 18 09 20 | 125 | yes | | |
| ne-208 | 16 06 05.7 | 18 16 43 | 125 | yes | | |
| ne-240 | 16 05 58.1 | 18 24 41 | 262 | conf. | | |
| ne-250 | 16 05 52.2 | 18 27 58 | 307 | yes | | |
| ne-398 | 16 04 18.0 | 18 14 06 | 352 | weak | | |
| ce-042 | 16 06 00.1 | 17 45 54 | 216: | yes | *B*, *V*, *i* | yes |
| ce-048 | 16 05 55.7 | 17 42 39 | 171 | conf. | *B*, *V*, *i* | yes |
| ce-060 | 16 05 44.6 | 17 42 19 | 171 | conf. | *B*, *V*, *i* | no |
| ce-061 | 16 05 41.1 | 17 48 00 | 216 | conf | *B*, *V*, *i* | yes |
| ce-143 | 16 05 20.6 | 17 52 02 | 171 | yes | *V*, *i* | yes |
| ce-176 | 16 05 09.9 | 17 51 20 | 171 | yes | *B*, *V*, *i* | yes |
| ce-200 | 16 05 06.7 | 17 47 00 | 216 | conf. | *B*, *V*, *i* | yes |
| sw-103 | 16 04 00.6 | 17 15 13 | 261 | yes | *B*, *V*, *i* | |
| sw-194 | 16 01 07.1 | 17 20 16 | 395 | – | *B*, *V*, *i* | |
| sw-222 | 16 03 05.8 | 17 10 14 | 261 | yes | *V*, *i* | yes |
| 47-138 | 16 00 17.5 | 15 53 15 | 216 | – | | |
| 47-154 | 16 02 26.6 | 15 57 36 | 372 | no | | |
| 47-166 | 16 02 16.2 | 16 04 41 | 261 | yes | | |
| 47-211 | 16 01 55.8 | 15 42 29 | 261 | yes | | |

Arecibo H I data: conf. indicates a spectrum confused by nearby galaxies,
– Objects for which no sensitive spectra could be obtained (see Sect. 3.1).

and *i* imaging could be obtained. Observations were carried out with the Wide Field Camera attached to the prime focus of the 2.5 m Isaac Newton Telescope (INT) of the Observatorio del Roque de los Muchachos, in Spain, on June 5, 1999 and April 26, 2000. Both fields were observed under photometric conditions. The WFC consists of a science array of four thinned AR coated EEV 4k × 2k devices, plus a fifth used for autoguiding. The pixel scale is 0.33 arcsec pixel$^{-1}$, which gives a total field of view of about 34′ × 34′. Given the particular arrangement of the detectors, an area of about 11′ × 11′ is not usable at the top right corner of the field.

The accuracy of the photometry is about 0.10 mag. For the *i*-band frames, the accuracy is slightly poorer due to residual fringing and the uncertainties of the colour term $\delta(V-i)$ is about 0.15 mag. Although a Sloan-Gunn *i* filter was used instead of Cousin *I*, the reported *I* magnitudes correspond to the Cousin system, as photometric standards from Landolt (1992) were observed and a linear relationship with a slope unity was found between the expected number of counts for each of the filters. The astrometry of the images was carried out using USNO guide stars. Detailed *V*-band images as well as $(V - I)$ colour maps are shown in Sect. 3.2.

**Table 2.** Journal of the optical spectroscopic observations.

| Object | Date | Telescope | PA[a] | Width[b] |
|---|---|---|---|---|
| ce-042 | April 28 2001 | NOT | 5.6 | 1.0 |
| ce-048 | June 19 2000 | WHT | 336.4 | 1.0 |
| ce-060 | March 19 2001 | NOT | 319.3 | 1.0 |
| ce-061 | June 19 2000 | WHT | 96.6 | 1.1 |
| ce-143 | July 11 2000 | WHT | 51.5 | 1.0 |
| ce-176 | April 26 2000 | WHT | 317.5 | 1.1 |
| ce-200 | March 19 2001 | NOT | 70.7 | 1.0 |
| sw-222 | May 14 2001 | NOT | 81.0 | 1.0 |

[a] In degrees, from North towards East.
[b] Width of the slit, in arcsecs.

### 2.3.2. Optical spectroscopy

Medium and low-resolution spectroscopy was carried out at the 4.2 m William Herschel Telescope (WHT) and the 2.5 m Nordic Optical Telescope (NOT) at the Observatorio del Roque de los Muchachos, in Spain. Table 2 shows the diary of the

spectroscopic observations. Observations at the WHT were performed during several nights using the double arm spectrograph ISIS, with the dichroic splitting the beam set at 5700 Å. For most of the galaxies observed at the WHT, the CCD set-up was two 1k × 1k Tektronix per arm. The gratings used were R300B and R316R, giving nominal dispersions of 1.54 Å pix$^{-1}$ and 1.49 Å pix$^{-1}$ for the blue and red arms, respectively. The corresponding spectral coverages were 3735–5311 Å and 6118–7643 Å, respectively, and the spatial scale in both detectors was 0.36 arcsec pix$^{-1}$. Note that ce-143 was observed with a different set-up, using a EEV 2k × 4k detector on the blue arm, giving a nominal dispersion of 0.86 Å pix$^{-1}$ and a spatial scale of 0.2 arcsec pix$^{-1}$. In all cases, the slit width was set to match the seeing, about 1.″0 for most of the objects. Observations at the NOT were taken using the faint object spectrograph ALFOSC, with a 2k × 2k LORAL detector and Grism #4, giving a nominal dispersion of 3.3 Å pix$^{-1}$. The total wavelength coverage with this set-up was 3200–9100 Å, and the spatial scale was 0.18 arcsec pix$^{-1}$.

The slit was always centred on the galaxy nucleus and positioned along the position angle of the major axis, as listed in Table 2. Although spectro-photometric standard stars were observed for flux calibration, only the relative fluxes of the emission lines are reliable, since several nights were non-photometric.

The emission lines were measured with the SPLOT package running on IRAF. For each emission line five independent measures were performed, and the adopted fluxes and errors are, respectively, the average and standard deviation of the five measures. For ce-042, ce-200 and sw-222 the intensities of the [NII] doublet and the H$\alpha$ line were determined by fitting the non-resolved triplet with three Gaussians. Similarly, the fluxes of the [SII] lines of sw-222 were obtained by fitting the doublet with two Gaussians. Larger errors resulted from this deblending process. No correction was made for line absorption in the Balmer lines. Only ce-200 shows an absorption feature at H$\beta$, for which we simply measured the intensity from the base of the emission line. For some of the spectra obtained at the WHT, we had to rescale the red part in order to get the same continuum levels at both sides of the gap, since it is well established that the continuum of HII regions/galaxies is smooth at these wavelengths. All lines were dereddened using the extinction coefficient derived from the Balmer decrement H$\alpha$/H$\beta$ and assuming a theoretical value for the intrinsic line ratio of 2.89 (Brocklehurst 1971). No extinction correction was applied to galaxies for which the observed H$\alpha$/H$\beta$ flux ratio was consistent with this value, within the errors.

## 3. Results

### 3.1. H I properties

The Arecibo H I spectra of the 20 galaxies for which we could obtain sensitive spectra are shown in Fig. 1, smoothed to a resolution of 9.1 km s$^{-1}$ for most objects, and to 19.5 km s$^{-1}$ for the weak line signal of ne-398 and for the undetected object 47-154. Not shown are the spectra of sw-194 and 47-138, for which no sensitive H I observations could be obtained due to the proximity of strong continuum sources.

Besides the VLA data of D97, on which the present study is based, published H I detections (see Appendix A) were only found for the merger system IC 1182, which contains the ce-061 tidal dwarf galaxy in one of its tails.

We compared (Table 3) the Arecibo global H I profile parameters to those of the D97 VLA observations, which have a synthesized beam size (HPBW) varying from 20″ × 21″ to 26″ × 29″, a velocity resolution of 44.2 km s$^{-1}$ (degraded to 88 km s$^{-1}$ for the determination of the profile parameters), an rms noise of about 0.13 mJy/beam per channel map at the centre of the primary beam, and a pixel size of 6″ × 6″, i.e. about 24 pixels per synthesized beam. Values in brackets indicate the 4 Arecibo profiles estimated to be significantly confused by line emission from nearby galaxies: ne-240, ce-048, ce-060 and ce-200 (see Appendix A for comments on these objects). Listed in the columns are the following data; note that all radial velocities in this paper, both optical and H I, are in the heliocentric system, using the conventional optical definition ($V = c(\lambda - \lambda_0)/\lambda_0$): (1) the galaxy's name, from D97, (2) the centre velocity of the VLA profile, $V_{\rm HI}$, (3) the width of the VLA profile at 50% of the maximum flux density, $W_{50}$, (4) the $I_{\rm H}$ integrated VLA H I line flux (see the description below), (5) the $I_{\rm ext}$ integrated VLA H I line flux (see the description below), (6) the centre velocity of the Arecibo H I profile, $V_{\rm HI}$, (7) the width of the Arecibo profile at 50% of the maximum flux density, $W_{50}$, (8) the width of the Arecibo profile at 20% of the maximum flux density, $W_{20}$, (9) the integrated Arecibo H I line flux, $I_{\rm HI}$ and (10) the rms noise levels of the Arecibo spectra.

As it is in principle not straightforward to determine the integrated H I line profiles parameters of faint objects from interferometric data, four different methods were used in D97. We converted the H I masses listed in D97 to integrated H I line fluxes assuming the cluster distance of 110.5 Mpc adopted in D97. The characteristics of these methods are as follows: $I_{\rm H}$ is the line flux measured by integrating the spectra over the group of contiguous pixels above threshold, $I_{\rm ext}$ is the line flux integrated over a larger area, estimated by statistical tests to contain the total line emission, while $I_{\rm peak}$ and $I_{\rm int}$ are obtained by fitting a two-dimensional Gaussian to the velocity-integrated H I column density map, where $I_{\rm peak}$ corresponds to the line flux within the central beam area and $I_{\rm int}$ to the integrated flux of the Gaussian. The latter is notoriously unstable.

Although observations with a single dish telescope like Arecibo result in only one spectrum per pointing position and the derivation of integrated H I profile parameters is straightforward, these profiles depend on the instrument's beam pattern, which can lead to confusion with other objects in the beam (see Appendix A), and single-dish data are more sensitive to RFI than interferometric data.

We estimated the uncertainties, $\sigma_{V_{\rm HI}}$, in the central H I velocities of the Arecibo line profiles, following Fouqué et al. (1990):

$$\sigma_{V_{\rm HI}} = 4R^{0.5}P_W^{0.5}X^{-1}\ [\mathrm{km\,s^{-1}}] \quad (1)$$

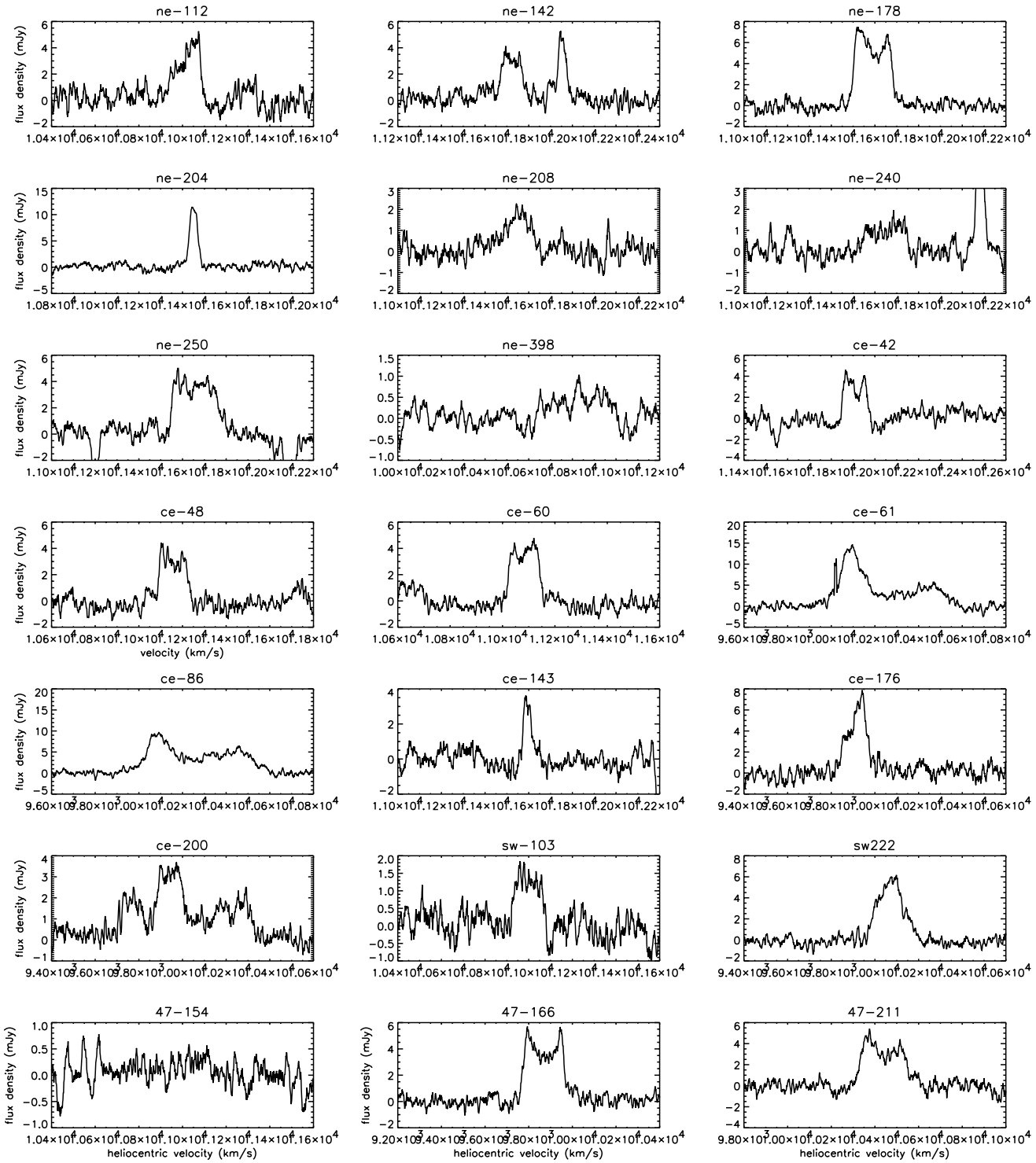


**Fig. 1.** Arecibo 21 cm H I line spectra of 20 galaxies in the Hercules cluster; for details on the ce-61 and ce-86 sources, see comments on ce-061 (Appendix A). The velocity resolution of the data is 9.1 km s$^{-1}$ for most spectra, and 19.4 km s$^{-1}$ for ne-398 and 47-154.

where $R$ is the velocity resolution in km s$^{-1}$, $P_W = (W_{20}-W_{50})/2$ in km s$^{-1}$ and $X$ is the signal-to-noise ratio of a spectrum, which we defined as the ratio of the peak flux density and the rms noise. The estimated uncertainties vary from 2 to 14 km s$^{-1}$ and are on average $4.6 \pm 2.5$ km s$^{-1}$. According to Fouqué et al., the uncertainty in the line widths is $2\sigma_{V_{\rm HI}}$ for $W_{50}$ and $3\sigma_{V_{\rm HI}}$ for $W_{20}$.

For the 13 objects for which an unambiguous comparison between the integrated Arecibo and VLA line fluxes can be made (see Table 1) the average ratio, and its $\sigma_{\rm N}$ deviation, between the two VLA flux determinations made without fitting a Gaussian to the source, $I_{\rm H}$ and $I_{\rm ext}$, and the Arecibo flux, $I_{\rm HI}$, is $I_{\rm H} = 0.66 \pm 0.27\ I_{\rm HI}$ and $I_{\rm ext} = 1.03 \pm 0.47 I_{\rm HI}$.

**Table 3.** Comparison of basic VLA and Arecibo H I observational data.

| | VLA data | | | | Arecibo data | | | | |
|---|---|---|---|---|---|---|---|---|---|
| Name | $V_{HI}$ | $W_{50}$ | $I_H$ | $I_{ext}$ | $V_{HI}$ | $W_{50}$ | $W_{20}$ | $I_{HI}$ | rms |
| | km s$^{-1}$ | km s$^{-1}$ | Jy km s$^{-1}$ | | km s$^{-1}$ | km s$^{-1}$ | km s$^{-1}$ | Jy km s$^{-1}$ | mJy |
| ne-112 | 11 046 | 262 | 0.23 | 0.24 | 11 014 ± 6 | 156 | 188 | 0.49 ± 0.09 | 0.63 |
| ne-142 | 11 711 | 171 | 0.19 | 0.36 | 11 726 ± 5 | 128 | 153 | 0.35 ± 0.07 | 0.47 |
| ne-178 | 11 556 | 217 | 0.63 | 0.92 | 11 591 ± 4 | 191 | 242 | 1.10 ± 0.09 | 0.49 |
| ne-204 | 11 467 | 125 | 0.56 | 0.70 | 11 451 ± 3 | 62 | 93 | 0.54 ± 0.06 | 0.60 |
| ne-208 | 11 556 | 125 | 0.10 | 0.20 | 11 521 ± 7 | 218 | 244 | 0.25 ± 0.07 | 0.39 |
| ne-240 | 11 645 | 262 | 0.18 | 0.32 | (11 636 ± 6 | 233 | 241 | 0.21) | 20.39 |
| ne-250 | 11 645 | 307 | 0.88 | 1.32 | 11 686 ± 5 | 283 | 307 | 0.84 ± 0.08 | 0.39 |
| ne-398 | 10 602 | 352 | 0.50 | 1.45 | 10 820 ± 14 | 364 | 377 | 0.15 ± 0.06 | 0.22 |
| ce-042 | 11 919: | 216: | 0.46: | 0.67: | 11 910 ± 3 | 127 | 135 | 0.33 ± 0.07 | 0.54 |
| ce-048 | 11 145 | 171 | 0.20 | 0.36 | (11 134 ± 2 | 208 | 211 | 0.53) | 0. 1 |
| ce-060 | 11 100 | 171 | 0.27 | 0.41 | (11 085 ± 4 | 130 | 150 | 0.51) | 0. 9 |
| ce-061 | 10 104 | 216 | 3.16 | 3.44 | 10 263 ± 3 | 595 | 666 | 3.44 ± 0.18 | 0.76 |
| ce-143 | 11 587 | 171 | 0.16 | 0.31 | 11 603 ± 3 | 95 | 101 | 0.14 ± 0.04 | 0.40 |
| ce-176 | 9905 | 171 | 0.43 | 0.51 | 9919 ± 4 | 150 | 183 | 0.65 ± 0.08 | 0.56 |
| ce-200 | 9927 | 216 | 0.10 | 0.17 | (9938 ± 4: | 177: | 189 | 0.46:) | 0.43 |
| sw-103 | 11 021 | 261 | 0.15 | 0.24 | 10 999 ± 4 | 155 | 159 | 0.18 ± 0.06 | 0.38 |
| sw-222 | 10 093 | 261 | 0.25 | 0.49 | 10 076 ± 4 | 192 | 226 | 0.79 ± 0.09 | 0.50 |
| 47-154 | 10 633 | 372 | 0.12 | 0.14 | – | | | | 0.32 |
| 47-166 | 9849 | 261 | 0.45 | 0.62 | 9887 ± 3 | 248 | 293 | 0.84 ± 0.06 | 0.35 |
| 47-211 | 10 423 | 261 | 0.30 | 0.58 | 10 460 ± 3 | 280 | 295 | 0.83 ± 0.10 | 0.51 |

Arecibo H I line parameters in brackets are for objects with profiles confused by nearby objects.

We also estimated the uncertainties, $\sigma_{I_{HI}}$, in the integrated line fluxes of the Arecibo line profiles following Fouqué et al. (1990), assuming that this formula, which was developed for Nançay data, can be applied to Arecibo data as well:

$$\sigma_{I_{HI}} = 5R^{0.5} I_{HI}^{0.5} h^{0.5} X^{-1} \text{ [Jy km s}^{-1}\text{]} \quad (2)$$

where $R$ and $X$ are as in Eq. (1) and $h$ is the peak flux density of the profile, in Jy. For the 13 abovementioned galaxies the estimated uncertainties vary between 5 and 30% of $I_{HI}$ and are on average $(0.16 \pm 0.08) \times I_{HI}$.

A comparison of the $W_{50}$ line widths measured with the VLA, which were used for the galaxy selection, and at Arecibo (Fig. 2) clearly shows the effect of the difference in velocity resolution, 88 and 9 km s$^{-1}$, respectively. It appears that, on average, the VLA line widths have been overestimated by about half a VLA channel width, i.e. 20 km s$^{-1}$.

Table 4 shows a summary of the H I properties of the sample galaxies as well as the absolute $B$ magnitudes of their optical counterparts. Listed in the columns of this Table are the following data: (1) the galaxy name, from D97, (2) the central radial velocity of the H I profile, $V_{HI}$, (3) the global form of the Arecibo spectra that are not confused, where DH denotes a double-horned profile, FT a flat topped one, G a Gaussian one and LS a lopsided profile, (4) the total H I mass, $M_{HI}$, (5) the relative H I gas content, $M_{HI}/L_B$, (6) the FWHM of the H I line, $W_{50}$, and (7) the absolute magnitude in the $B$ band, $M_B$, from NED. For the H I-related properties we preferentially used our Arecibo spectra, except for cases of confusion with nearby galaxies or a nearby strong continuum source, where we adopted the D97 VLA data, using the $I_{ext}$ estimate for the integrated line flux.

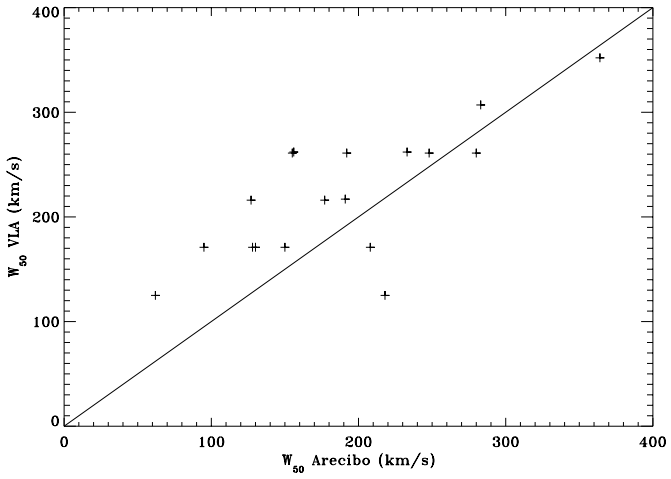


**Fig. 2.** Comparison of $W_{50}$ line widths of integrated H I profiles measured at Arecibo and the VLA, see the text for details. To guide the eye, a line with slope of unity has been plotted; it does not represent a fit to the data.

**Table 4.** Basic properties of the sample galaxies.

| Ident. | $V_{\rm HI}$ km s$^{-1}$ | Spec. form[a] | $M_{\rm HI}$ $10^9$ $M_\odot$ | $M_{\rm HI}/L_B$ $M_\odot/L_{\odot,B}$ | $W_{50}$ km s$^{-1}$ | $M_B$ mag |
|---|---|---|---|---|---|---|
| ne-112 | 11 014 | LS | 1.7 | 0.24 | 156 | −19.1 |
| ne-142 | 11 726 | FT | 1.8 | 3.7 | 128 | −16.2 |
| ne-178 | 11 591 | DH | 5.8 | 0.56 | 191 | −19.5 |
| ne-204 | 11 451 | G | 2.9 | 6.8 | 62 | −16.0 |
| ne-208 | 11 521 | G | 1.3 | 1.1 | 218 | −17.1 |
| ne-240 | (11 645) | – | (1.7) | (1.5) | (262) | −18.2 |
| ne-250 | 11 686 | FT | 4.4 | 0.96 | 283 | −19.8 |
| ne-398 | – | – | – | – | – | −16.3 |
| ce-042 | 11 910 | DH | 1.7 | 0.51 | 127 | −17.2 |
| ce-048 | (11 145) | – | (1.9) | (3.5) | (171) | −15.4 |
| ce-060 | (11 100) | – | (2.2) | (2.1) | (171) | – |
| ce-061 | (10 104) | – | (18.2) | (7.3) | (216) | – |
| ce-143 | 11 603 | G | 0.74 | 0.35: | 95 | −18.0 |
| ce-176 | 9919 | LS | 3.4 | 1.0 | 150 | −18.3 |
| ce-200 | (9938) | – | (0.90) | (0.43) | (216) | −17.6 |
| sw-103 | 10 999 | DH | 0.95 | 1.1 | 155 | −16.8 |
| sw-194 | (10 159) | – | (2.0) | 15.7: | (395) | −14.8 |
| sw-222 | 10076 | G | 4.2 | 0.35: | 192 | −19.8 |
| 47-138 | (11 284) | – | (1.2) | 0.30 | (216) | −18.4 |
| 47-154 | (10 633) | – | (0.74) | – | (372) | – |
| 47-166 | 9887 | DH | 4.4 | 1.4 | 248 | −15.0 |
| 47-211 | 10 460 | DH | 4.4 | 0.41 | 280 | −19.8 |

[a] The H I spectrum forms are: DH double horned, FT flat topped, G Gaussian, and LS lop-sided.

As mentioned above, the reported VLA H I detections of two of the galaxies – ne-398 and 47-154 – were not confirmed at Arecibo.

### 3.2. Optical properties

In this section we study the results obtained for the subsample for which we obtained optical spectra and/or imaging. Figures 3a, b show our *V*-band images of the ce and sw fields, respectively, with superimposed contours showing the H I clouds detected in D97. Figure 4 displays the optical spectra of all galaxies with emission lines and Table 6 lists their spectro-photometric data. Uncertainties derived from the deblending process for the [N II] and [S II] lines of the galaxies observed at the NOT are not included in the table.

#### 3.2.1. Structural properties

In Table 5 we list the absolute magnitudes and colours obtained for the 10 objects of the optical subsample, including the two tentative detections sw-103 and sw-194. For the seven galaxies which show optical emission lines, the magnitudes are extinction corrected using the $C(\mathrm{H}\beta)$ values listed in Table 6. The magnitudes listed in this table will be used hereafter for this subsample of galaxies.

For the surface photometry analysis we employed improved versions of the techniques described in Papaderos et al. (1996). Before determining the profiles we removed foreground stars and background galaxies intersecting the H I galaxies and smoothed all images of a given object to the same resolution. Surface brightness profiles (SBPs) were corrected for extinction inside the galaxies using the $C(\mathrm{H}\beta)$ values listed in Table 6.

In Table 7 we summarize the derived photometric properties. Listed in the 12 columns of this table are the following data: (1) the parameters $b$ and $q$, describing, respectively, the intensity distribution of the latter fitting formula near the centre, (3 and 4) the central surface brightness, $\mu_{\rm E,0}$, and exponential scale-length $\alpha$, respectively, of the Low Surface Brightness (LSB) component, as obtained from linear fits to the exponential regime of each profile and weighted by the photometric uncertainty of each point – note that Eq. (22) in Papaderos et al. (1996) predicts for the LSB component an actual central surface brightness $2.5\log(1-q)$ mag fainter than the extrapolated value $\mu_{\rm E,0}$, listed in Col. 3, (5) the corresponding total magnitude of the LSB component as obtained for a pure

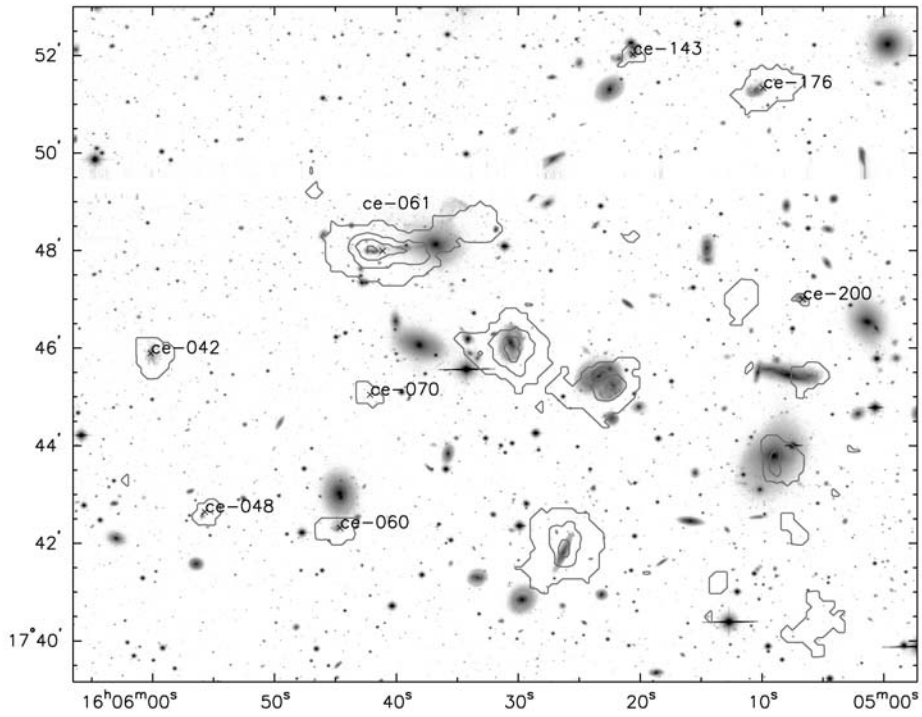


**Fig. 3. a)** VLA H I column density contours superposed on our optical *V*-band image of field ce. The labels indicate the H I-selected galaxies in this field. RA and Dec are in J2000. The HI cloud ce-070 reported by van Driel et al. (2003) is also labeled.

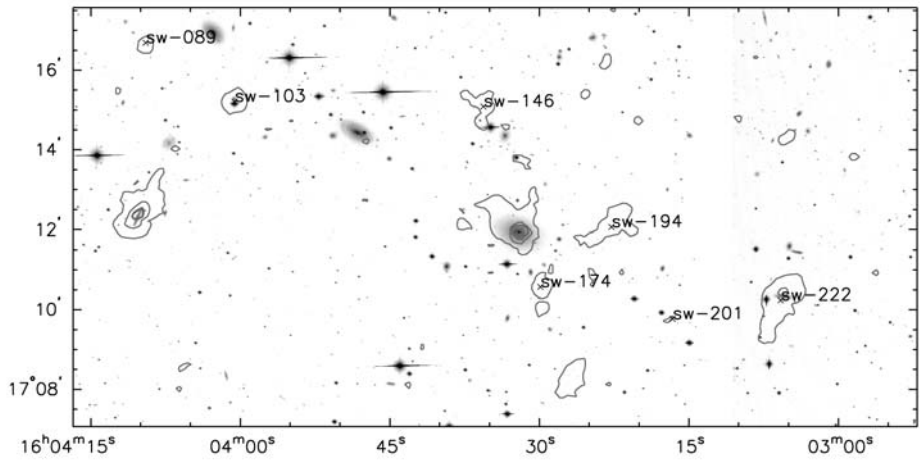


**Fig. 3. b)** VLA H I column density contours superposed on our optical *V*-band image of field sw. The labels indicate the H I-selected galaxies in this field. RA and Dec are in J2000. The HI clouds sw-089, sw-146 and sw-201 reported by van Driel et al. (2003) are also labeled.

or a modified exponential distribution, (6–9) list quantities obtained from profile decompositions; in (8) and (6) are listed, respectively, the isophotal radii $E_{25}$ and $P_{25}$ of the LSB component and of the luminosity component in excess of it, both determined at the 25 mag arcsec$^{-2}$ level, while in (9) and (7) are listed, respectively, the corresponding apparent magnitude of these components, $m_{E25}$ and $m_{P25}$, (10) the total apparent magnitude, as inferred from the SBP integration out to the last point, $m_{\rm SBP}$, (11) the effective radius, $r_{\rm eff}$, and the radius $r_{80}$, which encircles 80% of the galaxy's total flux, and (12) the Sérsic index $\eta$ resulting from fitting Eq. (5) in Papaderos et al. (1996) to the BSP.

*V*-band images, $(V-I)$ colour maps, surface brightness and colour profiles of the galaxies are presented in Figs. 5 to 12. A common property of all selected galaxies is the absence of notable colour gradients. In all cases these do not exceed 0.1 mag kpc$^{-1}$, as also reported for many dIs (e.g. Patterson & Thuan 1996; van Zee 2001). The situation is strikingly different in the inner regions ($R^* \lesssim E_{25}$) of BCDs, where colour gradients of up to $\gamma_+ \sim 1.8$ mag kpc$^{-1}$ have been observed, like H1034-2558 in the Hydra cluster (Paper I) and other examples in Papaderos et al. (1996a), Doublier et al. (1999) and Cairós et al. (2001).

For all galaxies except ce-061, an exponential fitting law provides a reasonable approximation to the SBPs in their outer low surface brightness regime. For half of the sample galaxies, however, inwards extrapolation of this outer exponential slope predicts a higher intensity than actually observed.

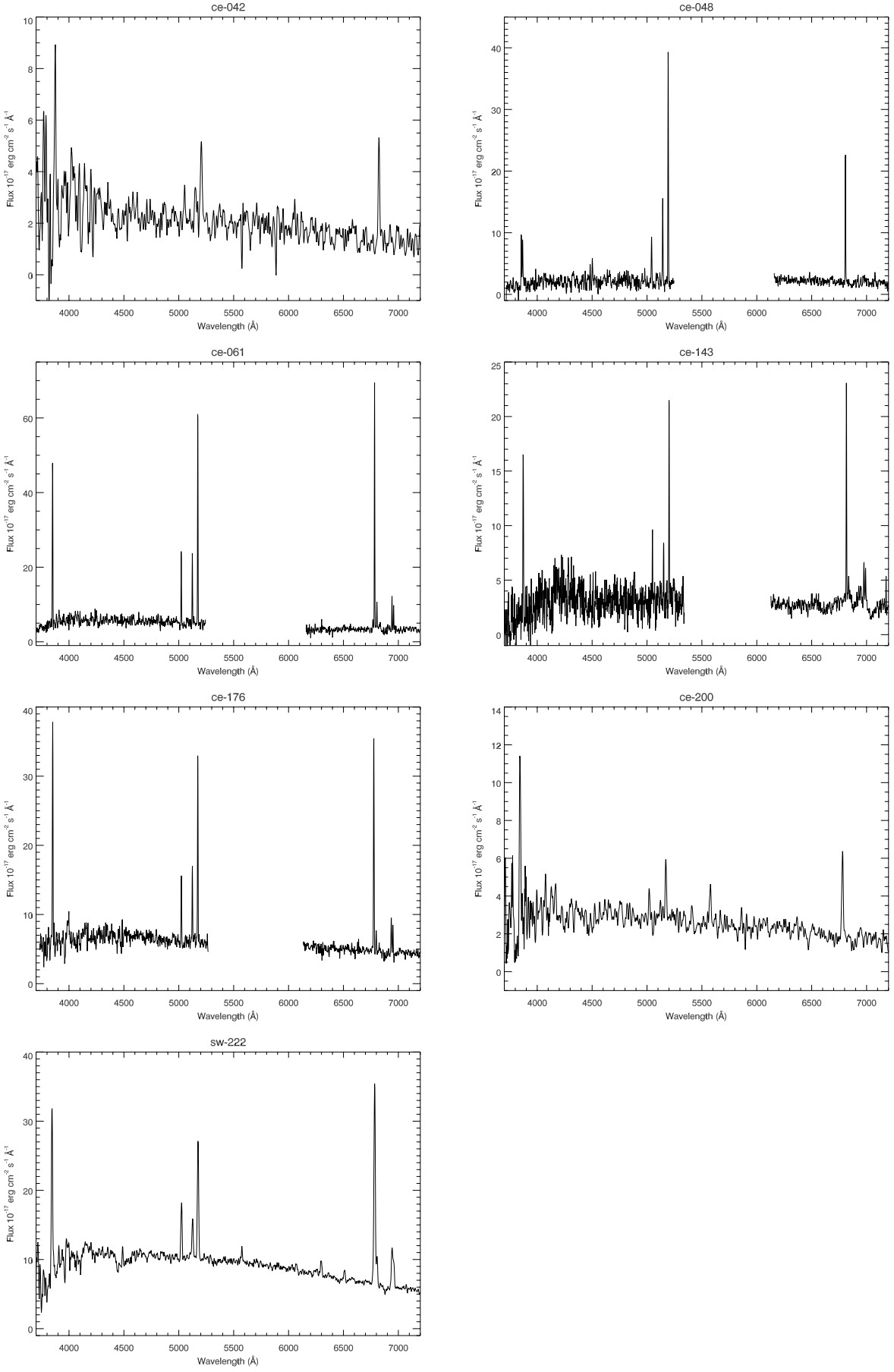


**Fig. 4.** Optical spectra of the seven galaxies showing emission lines.

**Table 5.** Absolute magnitudes and colours.

| Name | $M_V$ | $(B-V)$ | $(V-I)$ |
|---|---|---|---|
| ce-042 | −18.53 | 0.17 | 0.29 |
| ce-048 | −16.60 | 0.28 | 0.55 |
| ce-060 | −17.24 | 0.23 | 1.06 |
| ce-061 | −18.24 | 0.23 | 0.00 |
| ce-143 | −18.13† | – | 0.51 |
| ce-176 | −18.72 | 0.44 | 0.65 |
| ce-200 | −18.12 | 0.34 | 0.74 |
| sw-103 | −16.74 | – | – |
| sw-194 | −15.24 | – | 1.80 |
| sw-222 | −20.02† | – | 0.68 |

† The average $(B-V) = 0.3$ was assumed to estimate $M_B$.

This type of convex profile with an exponential distribution in the outer parts and levelling off in the inner part (within 1–3 disc scale lengths) is not rare among low-luminosity dwarf ellipticals (e.g. Binggeli & Cameron 1991), dwarf irregulars (Patterson & Thuan 1996; van Zee 2000), blue LSB galaxies (Rönnback & Bergvall 1994), near-infrared selected LSBs (Monnier Ragaigne et al. 2003), and has been reported in a few blue compact dwarfs (e.g., Fricke et al. 2001; Guseva et al. 2001; Vennik et al. 2000). Note that similar SBPs have also been derived for 4 of the H I-selected dwarfs in the Hydra cluster (H1031-2818, H1031-2632, H1032-2722 and H1033-2642; see Paper I). For those systems, following the procedure outlined in Guseva et al. (2001), we modelled the LSB component using Eq. (22) in Papaderos et al. (1996).

In Fig. 13 we show $M_B$ as function of $\mu_{0,B}$ for the Hercules and Hydra cluster galaxies. We used the average $(B-V)$ colour of 0.3 of the other galaxies in the subsample for ce-143 and sw-222, and included them in the plot. Also shown are the loci occupied by spiral discs, ellipticals and spiral bulges, dwarf Irregulars and dwarf ellipticals from Binggeli (1994), as well as the loci occupied by the LSB galaxies from van der Hulst (1998). All Hydra cluster galaxies and 5 of the 8 Hercules objects lie in the zone occupied by the faintest disc-like galaxies and by dwarf systems.

### 3.2.2. Star formation activity

Not surprisingly for an H I-selected sample, seven objects out of the eight for which we took optical spectra show emission lines, with line ratios typical of HII regions, indicating they are star-forming objects. The only quiescent galaxy is ce-060, which shows no sign of ongoing star formation. Unfortunately, non-photometric weather conditions did not allow us to derive a reliable star-formation rate from the H$\alpha$ luminosity.

In Fig. 14 we show the absolute blue magnitudes $M_B$ as function of the H$\beta$ equivalent widths for the Hercules and Hydra cluster galaxies. For comparison we have added the emission line galaxies from Salzer et al. (1989) as well as the upper envelope from Vílchez (1995). As can be seen from the figure, the Hercules cluster galaxies have H$\beta$ equivalent widths normal for their $B$-band luminosities, compared to the Salzer et al. sample, whereas the Hydra cluster dwarfs seem to delineate the lower envelope of the locus occupied by the Salzer et al. sample.

Broad-band colours can also be used as a diagnostic of star formation, and we show the $(B-V)$ vs. $(V-I)$ diagram for our sample galaxies in Fig. 15. For comparison, we have added the ellipticals from Goudfrooij et al. (1994), the spirals from Heraudeau & Simien (1996), the amorphous galaxies from Gallagher & Hunter (1987) and the nearby dwarfs from Makarova (1999) – the latter objects were defined by Sandage & Brucato (1979) as blue galaxies showing centrally concentrated light distributions, with a high H I gas content, low rotation velocities and heavy-element abundances typical of Magellanic Irregulars. We notice that all 7 of our Hercules cluster galaxies with both colours available are concentrated towards the bottom left region of the diagram, i.e. the blue part of the sequence delineated by the amorphous and dwarf samples, where no ellipticals and only a marginal number of spirals are found.

### 3.2.3. Metallicity

The H I-based selection process resulted in star–forming galaxies hosting H II regions of which the metallicity of the ionised gas could be estimated from their emission lines. As the [OIII]$\lambda$4363 Å line was not detected for any of the galaxies, the oxygen abundances were computed from the [OII]$\lambda$3727 Å and [OIII]$\lambda$4959,5007 Å emission line fluxes, using several abundance calibrations: the $R_{23}$ method calibrated theoretically by McGaugh et al. (1991), in its parameterised form from Kobulnicky et al. (1999), the more recent $p$-method (Pilyugin 2000, 2001) and the independent method of van Zee et al. (1998), based on the [NII]/H$\alpha$ line ratio. The first two methods each provide two possible values of the metallicity for a given observable. To resolve the degeneracy and choose between the lower and upper values, we relied on the strength of the [NII]/[OII] ratio (see van Zee et al. 1998). The values of $12 + \log(\mathrm{O/H})$ obtained with these three methods, as well as the final adopted values, are listed in Table 8.

The criteria used to choose the final adopted abundances listed in Col. 7 were the following: the abundances were preferably derived using the $p$-method, for consistency with previous work in this program (Paper II). Although the method based on [NII]/H$\alpha$ is not very reliable, because of blending problems of the H$\alpha$ and [NII] lines in the low resolution NOT spectra, it was preferred for those objects (ce-042 and ce-200, marked with a colon in Table 8) whose observed line fluxes are not within the validity range of the $p$-method, and which yield inconsistent metallicities: i.e. the oxygen abundance read on the lower branch is larger than that read on the upper branch.

The median oxygen abundance of these 7 Hercules cluster sample galaxies is about one third solar ($12 + \log(\mathrm{O/H}) = 8.27 \pm 0.31$), with a quite large scatter. Figure 16 shows their metallicities as function of absolute $B$ magnitude; the typical uncertainty in the oxygen abundances is indicated by the error

**Table 6.** Extinction-corrected emission line flux ratios with respect to H$\beta$[†].

| | ce-042 | ce-048 | ce-061 | ce-176 | ce-200 | ce-143 | sw-222 |
|---|---|---|---|---|---|---|---|
| [OII] $\lambda$3727 Å | 6.149 | 0.932 | 2.475 | 3.062 | 6.234 | 3.505 | 3.044 |
| | (1.108) | (0.050) | (0.122) | (0.343) | (0.956) | (0.322) | (0.154) |
| H$_\beta$ $\lambda$4861 Å | 1.000 | 1.000 | 1.000 | 1.000 | 1.000 | 1.000 | 1.000 |
| | (0.071) | (0.012) | (0.016) | (0.052) | (0.042) | (0.037) | (0.016) |
| [OIII] $\lambda$4959 Å | – | 1.424 | 0.940 | 1.004 | – | 0.834 | 0.597 |
| | – | (0.040) | (0.033) | (0.086) | – | (0.065) | (0.038) |
| [OIII] $\lambda$5007 Å | 2.955 | 3.559 | 2.753 | 2.287 | 1.878 | 2.730 | 1.867 |
| | (0.299) | (0.078) | (0.069) | (0.154) | (0.135) | (0.142) | (0.054) |
| [NII] $\lambda$6548 Å | 0.203 | – | 0.142 | – | 0.086 | – | 0.167 |
| | (0.080) | – | (0.009) | – | (0.063) | – | (0.015) |
| H$_\alpha$ $\lambda$6563 Å | 2.891 | 2.756 | 2.891 | 2.770 | 2.890 | 2.889 | 2.890 |
| | (0.528) | (0.108) | (0.105) | (0.334) | (0.344) | (0.277) | (0.109) |
| [NII] $\lambda$6584 Å | 0.466 | – | 0.332 | 0.298 | 0.186 | 0.447 | 0.407 |
| | (0.116) | – | (0.021) | (0.045) | (0.068) | (0.067) | (0.019) |
| [SII] $\lambda$6717 Å | – | – | 0.402 | 0.529 | – | 0.703 | 0.573 |
| | – | – | (0.022) | (0.066) | – | (0.096) | (0.026) |
| [SII] $\lambda$6731 Å | – | – | 0.300 | 0.365 | – | 0.513 | 0.371 |
| | – | – | (0.017) | (0.047) | – | (0.057) | (0.017) |
| $V_{\rm hel}$ (km s$^{-1}$) | 11 840 | 11 181 | 10 012 | 9875 | 9940 | 11 616 | 10 087 |
| | (90) | (39) | (76) | (95) | (65) | (63) | (20) |
| $C$(H$_\beta$) | 0.298 | 0.000 | 0.004 | 0.000 | 0.103 | 0.116 | 0.166 |
| | (0.117) | (0.025) | (0.023) | (0.077) | (0.076) | (0.061) | (0.024) |
| $EW$(H$_\beta$) (Å) | 10.4 | 47.7 | 30.9 | 14.3 | 8.9 | 13.0 | 14.5 |
| | (1.0) | (2.5) | (0.9) | (1.1) | (0.4) | (0.6) | (0.3) |

[†] Quantities in parenthesis correspond to the errors of the quantities quoted above.

bar. For the two galaxies without an available $B$ magnitude, ce-143 and sw-222, a ($B - V$) colour of 0.30 – the median value measured for the other Hercules cluster galaxies – was assumed. For comparison, we added the isolated dwarf Irregulars of Richer & McCall (1995), the LSBs from van der Hulst et al. (1998), the H I-selected dwarfs from the Hydra cluster (Paper II) and the tidal dwarf galaxies (TDGs) from Duc et al. (2000). The straight line represents the empirical relationship found by Richer & McCall (1995) for their dwarf sample.

The majority of the Hercules cluster galaxies show metallicities following the empirical relationship for Irregular dwarfs, taking into account the uncertainties. Exceptions are ce-042, which looks overabundant for its luminosity and lies well within the loci of the LSBs and the TDGs, and ce-048, with a metallicity lower than expected for its luminosity and whose spectrum resembles that of typical BCDs. The presence of a few over–metallic object was also reported in the Hydra cluster by Duc et al. (2001a). Unique among our objects in the Hercules cluster is the TDG ce-061 (Braine et al. 2001), whose dynamical nature as a gravitationally bound system inside the tidal tail of the IC 1182 merger system has been confirmed recently through H$\alpha$ line Fabry-Pérot imaging (Duc & Amram 2003).

### 3.2.4. The two tentative optical detections

Figures 17a, b show $V$-band contour plots of the two optical detections we tentatively associate with the VLA H I sources sw-103 and sw-194. The filled circles indicate the centre positions of the H I clouds. Although in both cases the difference in position between the centres of the optical and H I sources are small compared to the VLA beam size (see below), which favours their association, the physical link between the H I detections and the optical counterparts could not be proven unequivocally, as we could not obtain optical spectra for these two galaxies since they are too faint. Such optical spectra are needed to confirm their associations to the H I clouds.

Unfortunately, sw-103 is too close to a bright star for a detailed morphological analysis. The difference between the optical and H I centre is only about 4″, or one fifth of the VLA HPBW. Although its $V$-band magnitude could be

**Table 7.** Photometric results and structural properties of the galaxies with definite optical counterparts[a].

| Name | Band | $\mu_0$ | $\alpha$ | $m^{\rm fit}_{\rm LSB}$ | $P_{25}$ | $m_{P_{25}}$ | $E_{25}$ | $m_{E_{25}}$ | $m_{\rm SBP}$ | $r_{\rm eff}$,$r_{80}$ | $\eta$ |
|---|---|---|---|---|---|---|---|---|---|---|---|
| | | mag/□″ | kpc | mag | kpc | mag | kpc | mag | mag | kpc | |
| (1) | (2) | (3) | (4) | (5) | (6) | (7) | (8) | (9) | (10) | (11) | (12) |
| ce-042 | *B* | 21.25 ± 0.50 | 2.14 ± 0.23 | 17.67 | 2.96 | 19.35 | 7.14 | 18.06 | 17.50 | 4.35, 7.29 | 0.91 |
| *(2.8,0.9)* | *V* | 21.26 ± 0.45 | 2.24 ± 0.22 | 17.59 | 3.48 | 18.91 | 7.87 | 17.98 | 17.31 | 4.35, 7.36 | 0.91 |
| | *I* | 21.13 ± 0.52 | 2.32 ± 0.30 | 17.38 | 4.01 | 18.43 | 8.20 | 17.62 | 17.04 | 4.26, 7.31 | 0.85 |
| ce-048 | *B* | 22.68 ± 0.16 | 1.17 ± 0.06 | 19.61 | 1.06 | 22.25 | 2.49 | 20.11 | 19.52 | 1.65, 3.06 | 0.89 |
| ⋆ | *V* | 22.59 ± 0.15 | 1.19 ± 0.06 | 19.48 | 1.55 | 20.79 | 2.64 | 19.94 | 19.21 | 1.48, 2.87 | 0.77 |
| | *I* | 22.51 ± 0.34 | 1.23 ± 0.10 | 19.32 | 1.89 | 19.68 | 2.83 | 19.76 | 18.72 | 1.30, 2.56 | 0.62 |
| ce-060 | *B* | 23.42 ± 0.13 | 2.45 ± 0.13 | 18.74 | 0.89 | 23.00 | 3.56 | 19.67 | 18.85 | 3.26, 5.38 | 0.90 |
| ⋆ | *V* | 23.15 ± 0.10 | 2.41 ± 0.10 | 18.51 | 1.41 | 19.14 | 4.10 | 19.25 | 18.59 | 3.07, 5.21 | 0.87 |
| | *I* | 22.11 ± 0.13 | 2.44 ± 0.14 | 17.45 | 6.56 | 17.73 | 6.48 | 17.77 | 17.54 | 3.08, 5.23 | 0.83 |
| ce-061 | *B* | 22.68 ± 0.27 | 2.41 ± 0.19 | 18.72 | 3.87 | 18.46 | $<P_{25}$ | – | 17.84 | 2.70, 5.33 | 0.63 |
| *(2.4,0.88)* | *V* | 22.44 ± 0.23 | 2.38 ± 0.16 | 18.50 | 3.95 | 18.19 | 3.91 | 19.96 | 17.60 | 2.60, 5.21 | 0.61 |
| | *I* | 21.50 ± 0.42 | 2.19 ± 0.25 | 17.72 | 3.91 | 17.80 | 6.93 | 18.12 | 17.06 | 2.69, 5.52 | 0.63 |
| ce-143 | *V* | 21.32 ± 0.11 | 1.20 ± 0.04 | 18.2 | – | – | 4.08 | 18.36 | 18.32 | 2.07, 3.48 | 1.09 |
| ⋆ | *I* | 20.97 ± 0.13 | 1.24 ± 0.05 | 17.78 | – | – | 4.59 | 17.91 | 17.82 | 2.03, 3.42 | 0.99 |
| ce-176 | *B* | 21.89 ± 0.20 | 2.26 ± 0.10 | 17.69 | 2.01 | 20.39 | 6.45 | 18.06 | 17.54 | 4.22, 6.87 | 1.17 |
| *(2.1,0.7)* | *V* | 21.61 ± 0.17 | 2.35 ± 0.10 | 17.33 | 3.16 | 19.22 | 7.32 | 17.62 | 17.12 | 4.11, 6.83 | 1.09 |
| | *I* | 21.11 ± 0.31 | 2.41 ± 0.18 | 16.77 | 4.90 | 17.99 | 8.63 | 16.96 | 16.46 | 3.96, 6.71 | 1.00 |
| ce-200 | *B* | 20.35 ± 0.32 | 1.16 ± 0.07 | 18.31 | 2.26 | 19.89 | 4.94 | 18.52 | 18.07 | 2.59, 4.30 | 1.41 |
| *(3.3,0.92)* | *V* | 20.06 ± 0.21 | 1.16 ± 0.05 | 18.00 | 2.44 | 19.44 | 5.30 | 18.12 | 17.72 | 2.59, 4.30 | 1.39 |
| | *I* | 19.35 ± 0.09 | 1.18 ± 0.03 | 17.27 | 2.67 | 18.67 | 6.24 | 17.36 | 17.00 | 2.59, 4.37 | 1.23 |
| sw-222 | *V* | 20.31 ± 0.07 | 1.64 ± 0.03 | 16.51 | – | – | 7.08 | 16.59 | 16.42 | 2.55, 4.40 | 0.97 |
| ⋆ | *I* | 19.65 ± 0.08 | 1.65 ± 0.04 | 15.83 | – | – | 8.13 | 15.88 | 15.74 | 2.53, 4.42 | 0.91 |

*a*: All listed values are corrected for extinction assuming a $C(\mathrm{H}\beta)$ as listed in Table 6.

estimated ($m_V \approx 19.1$), this was not possible in the *I*-band due to the close bright star.

The other tentative case, sw-194, may well be spurious. It is noted in D97 that this VLA H I source could be an artefact due to a nearby strong continuum source (see Appendix A). It is clearly extended (about $1\farcm5 \times 0\farcm5$) and four galaxies (see Fig. 17b) lie within its contour. Our tentative identification concerns the brightest and largest of the four objects only, which lies about 11″ from the centre of the VLA source. It is a very faint galaxy, for which we estimated $m_V \approx 20.6$ and $(V-I) \approx 1.8$, which is redder than expected for an H I-rich galaxy. Although the three other objects are fainter and smaller, their association with the H I source remains possible.

## 4. Discussion

As mentioned earlier, one of our aims is the identification of H I-selected dwarf galaxies in clusters. Although different dwarf selection criteria based on the H I and optical properties of galaxies are used in the literature, there is no precise and universally accepted definition of what exactly a dwarf galaxy is (e.g., Binggeli 1994). The classification criteria we can apply to our data are: narrow H I line width, Gaussian H I line shape, faint optical luminosity and central surface brightness as a function of luminosity. Two galaxies, ne-398 and 47-154, could not be classified, as they were not detected in H I at Arecibo and therefore lack an accurate line width.

Despite having an optical morphology and structural parameters reminiscent of dwarf or low-luminosity galaxies, most of the H I-selected objects in our sample have rather large H I line widths and sometimes double-horn profile shapes that are inconsistent with them being low-mass objects.

The only two systems in our Hercules cluster sample that satisfy all four dwarf selection criteria are ne-204 and ce-143: both have a $W_{50}$ profile width smaller than 100 km s$^{-1}$, a Gaussian H I profile shape, an absolute blue luminosity fainter than −18 (see Table 4) and they lie among the dwarfs in Fig. 13.

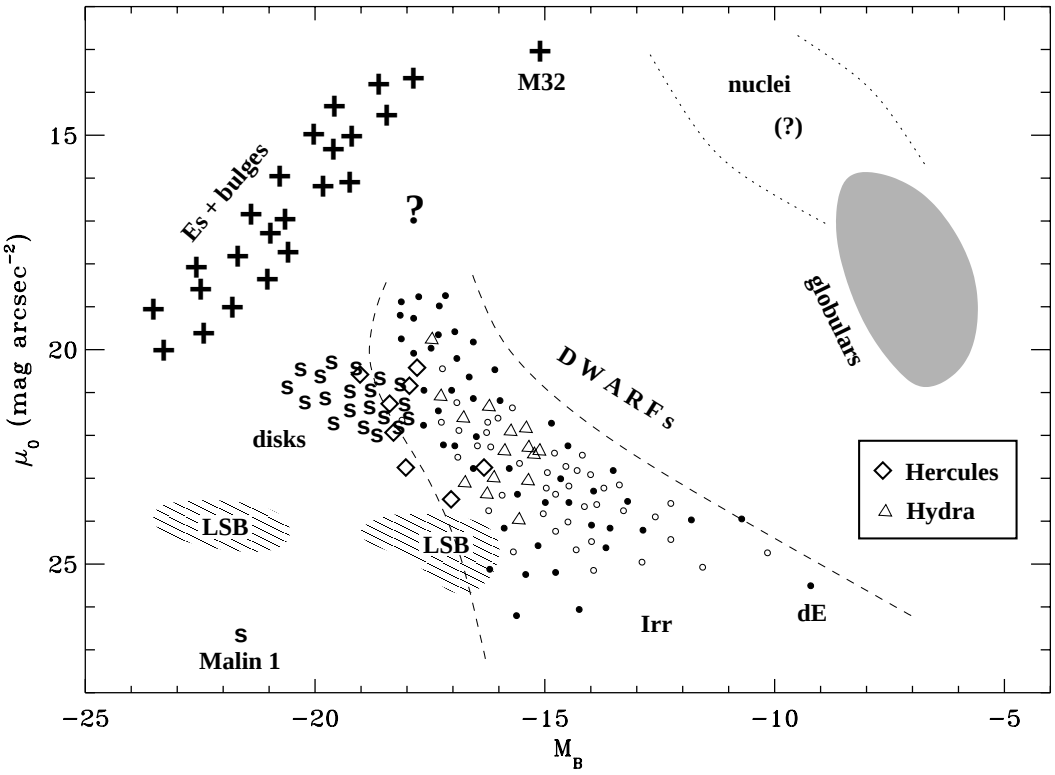


**Fig. 13.** Comparison of the absolute blue magnitude and blue central surface brightness of different types of galaxies and stellar subsystems, see text for details. To the original version of Binggeli (1994) the loci of the LSB galaxies from van der Hulst (1998) have been added, as well as the objects with available CCD surface photometry from our samples of H I-selected galaxies in the Hercules and Hydra clusters.

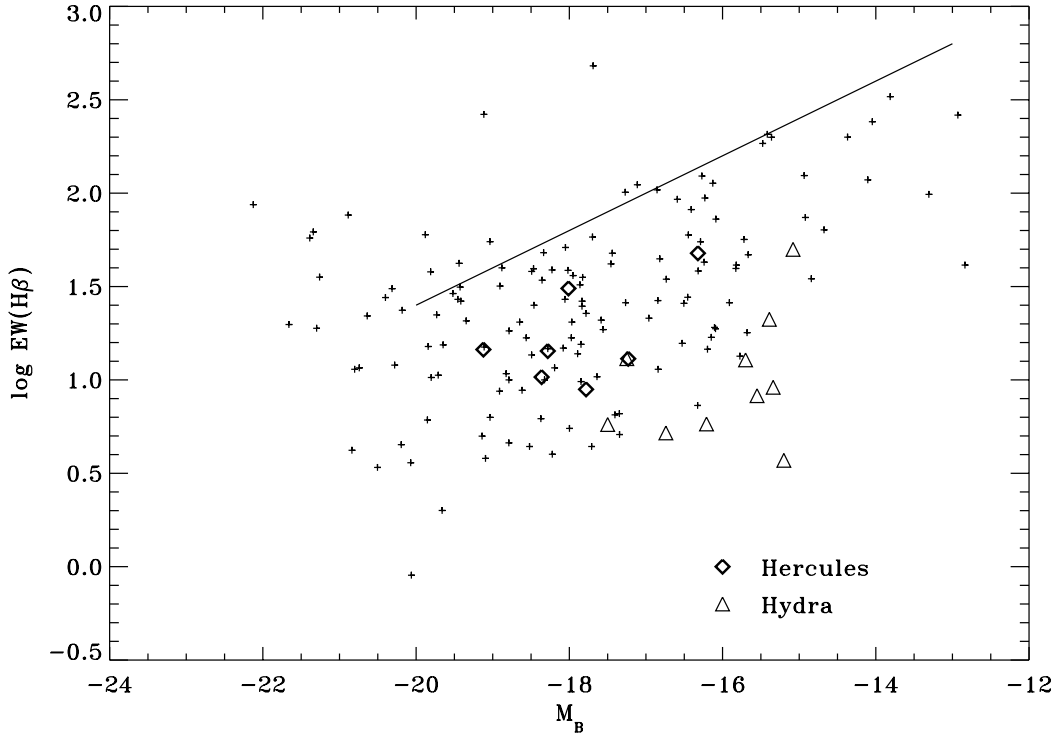


**Fig. 14.** Absolute blue magnitude as function of H$\beta$ equivalent width for the Hercules and Hydra cluster samples. For comparison we have added the emission line galaxies from Salzer et al. (1989), represented by small crosses. The straight line corresponds to the upper envelope from Vílchez (1995).

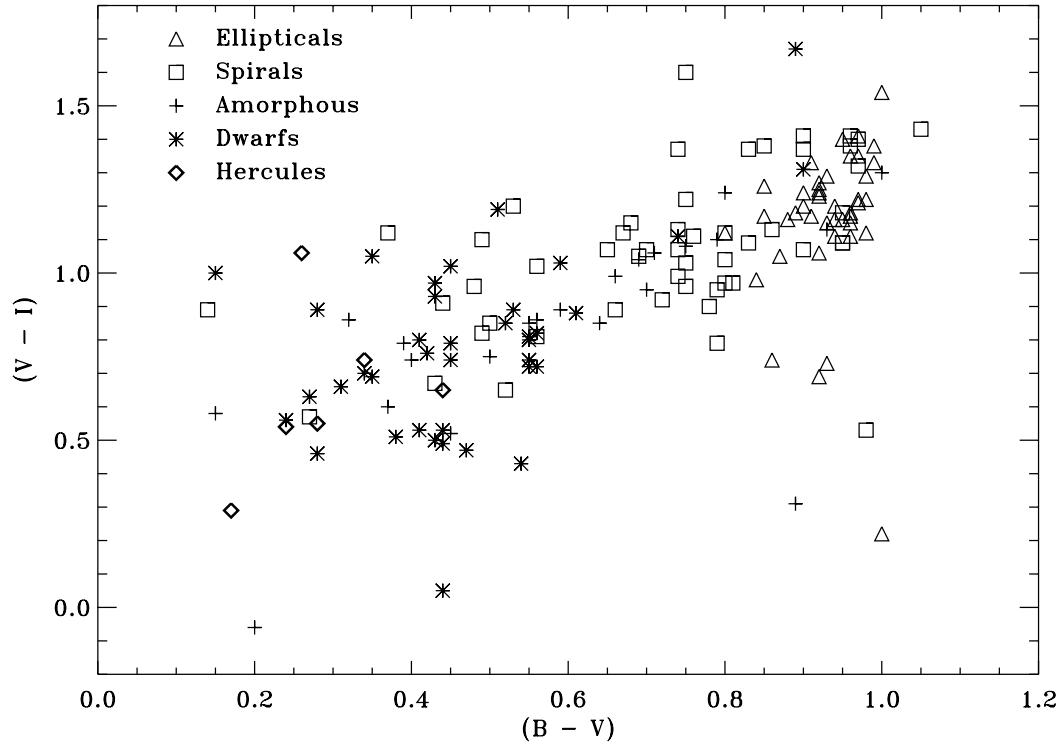


**Fig. 15.** ($B - V$) vs. ($V - I$) diagram for the Hercules cluster galaxies. Also shown are ellipticals from Goudfrooij et al. (1994), spirals from Heraudeau & Simien (1996), amorphous galaxies from Gallagher & Hunter (1987) and nearby dwarfs from Makarova (1999).

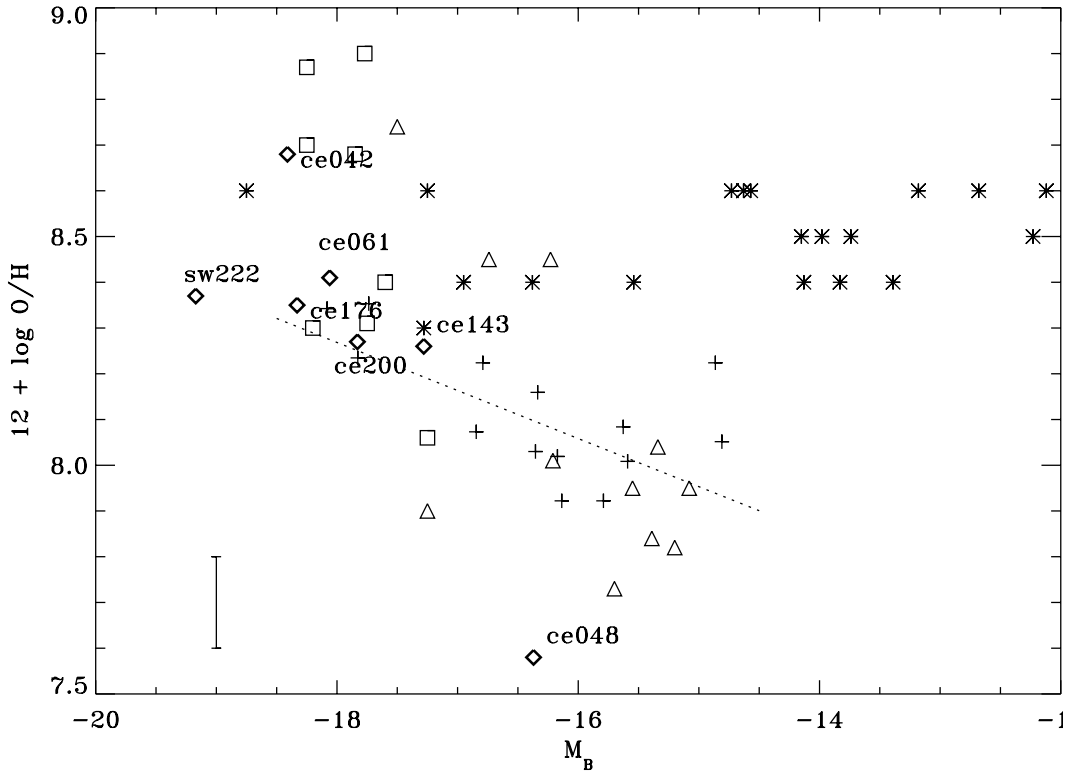


**Fig. 16.** Metallicity vs. luminosity relationship for the Hercules and Hydra cluster galaxies, represented by open diamonds and triangles respectively. The typical uncertainty in the metallicity determinations is represented by the error bar at the bottom left. Also shown are the sample of dwarfs from Richer & McCall (1995), the LSBs from van der Hulst et al. (1998) and the tidal dwarfs from Duc et al. (2000), represented by crosses, squares and asterisks, respectively.

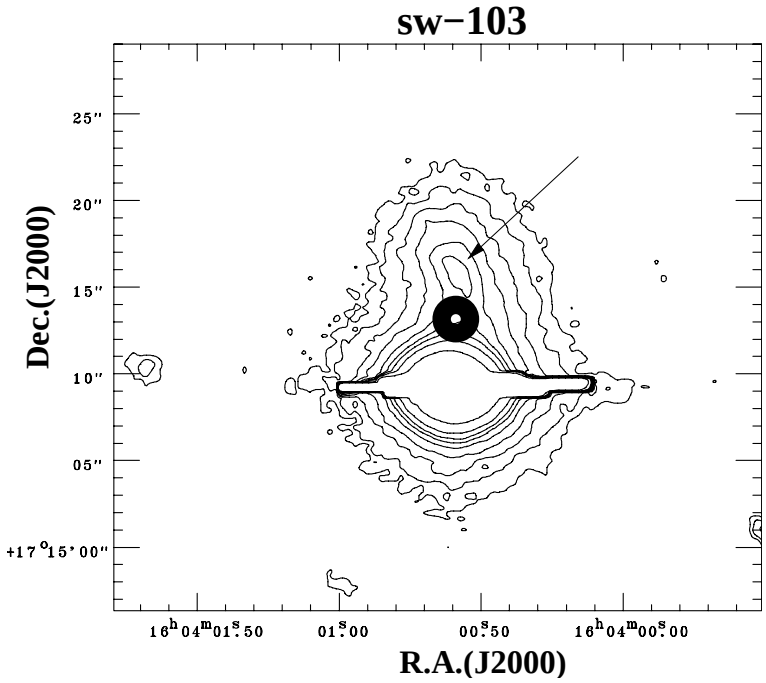


**Fig. 17. a)** *V*-band contour plot of the tentative detection corresponding to sw-103. Contour levels are 25.5, 24.5, 23.5, 22.5 and 21.5 mag arcsecs$^{-2}$. The filled circle shows the centre position of the VLA HI source from Dickey (1997).

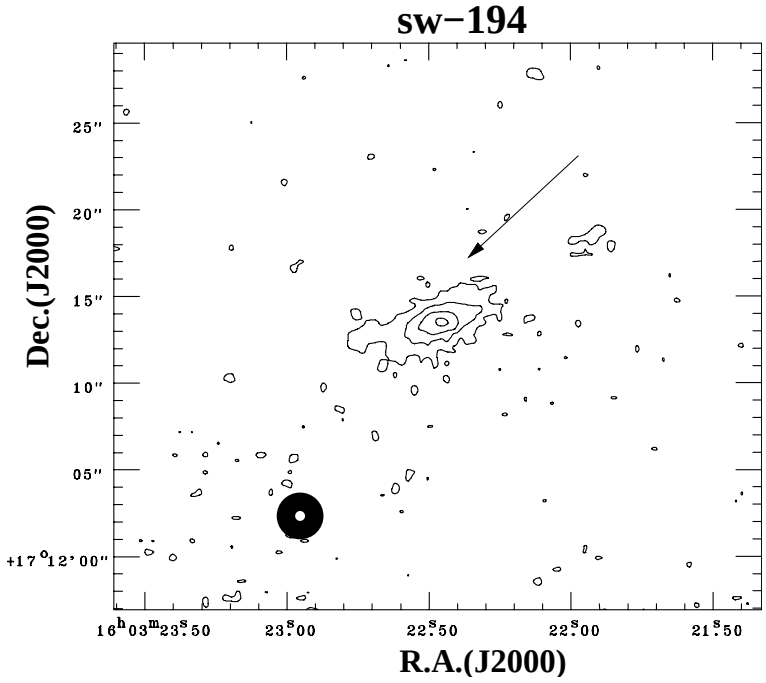


**Fig. 17. b)** *V*-band contour plot of the tentative detection corresponding to sw-194; we have assumed that the gas cloud is associated with the brightest galaxy in the field, 11″ W of the centre position (see Sects. 3.2.4 and 4). Contour levels are 25.5, 24.5, 23.5, 22.5 and 21.5 mag arcsecs$^{-2}$. The filled circle shows the position of the VLA HI source from Dickey (1997).

The levels of star formation in the four galaxies for which optical imaging and spectroscopy was obtained – as indicated by their H$\beta$ equivalent widths and optical colours – were found to be typical of those of active star-forming galaxies.

The metallicities of two objects do not follow the same trend as the five others: ce-042 was found to be overabundant for its luminosity and to lie well within the loci occupied by tidal dwarfs and LSBs, whereas ce-048 shows a very low metallicity for its luminosity. In fact, it is likely that the presence of a strong burst of star formation in ce-48, as its large H$\beta$ equivalent width suggests, has raised its luminosity, thus shifting it significantly in the *B*-band luminosity vs. metallicity diagram.

The presence of two gas clouds with tentative optical detections (sw-103 and sw-194) should also be noted. While the

**Table 8.** Oxygen abundances (12 + logO/H).

| Name | *p*-method | | $R_{23}$ | | N2Ha | Adopted |
|---|---|---|---|---|---|---|
| | low | up | low | up | | abundance |
| ce-042 | 8.52 | 7.91 | 8.49 | 8.24 | 8.68 | 8.68: |
| ce-048 | 7.58 | 8.61 | 7.73 | 8.71 | – | 7.58 |
| ce-061 | 7.88 | 8.41 | 7.98 | 8.62 | 8.53 | 8.41 |
| ce-176 | 8.02 | 8.35 | 8.03 | 8.60 | 8.48 | 8.35 |
| ce-200 | 8.66 | 7.94 | 8.43 | 8.31 | 8.27 | 8.27: |
| ce-143 | 8.10 | 8.26 | 8.14 | 8.51 | 8.66 | 8.26 |
| sw-222 | 8.03 | 8.37 | 7.99 | 8.64 | 8.62 | 8.37 |

former was confirmed in H I at Arecibo, the latter, which could not be observed at Arecibo, could be a spurious VLA detection, according to D97. If the optical counterparts are really physically associated to the neutral gas clouds, they would be dwarf galaxies according to their optical magnitudes of $M_B \sim -16.9$ and $-14.8$, respectively. If our tentative identification of a single galaxy with sw-194 were correct and the H I source not spurious (see Sect. 3.2.4), then its H I mass-to-blue luminosity ratio would be about 16 $M_\odot/L_{\odot,B}$, an unprecedented high value for a dwarf, while sw-103 would have a quite mundane ratio of 1.1 $M_\odot/L_{\odot,B}$. If the physical association between these H I and optical sources were not confirmed, we may be dealing with gas clouds without detected optical counterparts in a cluster, whose existence would impose constraints on the cluster properties.

Our accumulated data on the Hercules and Hydra cluster galaxies will be discussed further in a future paper on the influence of the cluster environment on galaxies, specifically dwarfs (Duc et al., in preparation).

## 5. Conclusions

According to various diagnostics, two of our sample galaxies (ce-143 and ne-204) can be classified as dwarfs. Of the galaxies studied in the optical, the star formation properties are similar to those of other samples of actively star forming galaxies and their metallicities are consistent with the blue luminosity-metallicity relation of nearby dwarfs, except for two galaxies, one of which is over-metallic and the other under-metallic for its luminosity. For two others the physical association with the H I clouds seen superimposed on them could not be proven, since no optical redshifts could be obtained. If confirmed, one of them (sw-194) would have an extremely high H I content. A particularly interesting object in our sample is located in the IC 1182 merger system: the Tidal Dwarf Galaxy ce-061, which shows a rather high luminosity, metallicity and H I content.

*Acknowledgements.* Some of the data presented here have been taken using ALFOSC, which is owned by the Instituto de Astrofísica de Andalucía (IAA) and operated at the Nordic Optical Telescope under agreement between IAA and the NBIfAFG of the Astronomical Observatory of Copenhagen. The NOT and WHT are operated on the island of La Palma by the NOT and ING groups, at the Observatorio del Roque de Los Muchachos of the Instituto de Astrofísica de Canarias. We also acknowledge the Service Program of the ING group for useful observations presented in this paper. We would like to thank the staff of Arecibo Observatory for their help with the observations and data reduction, especially P. Perrillat. IRAF, the Image Reduction and Analysis Facility, is written and supported at the National Optical Astronomy Observatory. We have made use of the NASA/IPAC Extragalactic Database (NED), which is operated by the Jet Propulsion Laboratory, California Institute of Technology, under contract with the National Aeronautics and Space Administration, and the Lyon-Meudon Extragalactic Database (LEDA). JIP acknowledges the Fifth Framework Program of the European Union for a Marie Curie Postdoctoral Fellowship. Research by PP has been supported by the Deutsches Zentrum für Luft– und Raumfahrt e.V. (DLR) under grant 50 OR 9907 7. C.B.F. WvD acknowledges the CNRS-SDU for travel support through the ASTE program.

## References

Barmby, P., & Huchra, J. P. 1998, AJ, 115, 6
Bieging, J. H., & Biermann, P. 1983, AJ, 88, 161
Binggeli, B., & Cameron, L. M. 1991, A&A, 252, 27
Binggeli, B. 1994, A note on the Definition and Nomenclature of Dwarf Galaxies, in Proc. ESO/OHP Workshop on Dwarf Galaxies, ed. G. Meylan, & P. Prugniel (ESO, Garching), 13
Bird, C. M., Dickey, J. M., & Salpeter, E. E. 1993, ApJ, 404, 81
Bothun, G. D., Stauffer, J. R., & Schommer, R. A. 1981, ApJ, 247, 42
Bothun, G. D., Aaronson, M., Schommer, R. A., et al. 1985, ApJS, 57, 423
Braine, J., Duc, P.-A., Lisenfeld, U., et al. 2001, A&A, 378, 51
Brocklehurst, M. 1971, MNRAS, 153, 471
Cairós, L. M., Vílchez, J. M., Gónzalez-Pérez, J. N., Iglesias-Páramo, J., & Caon, N. 2001, ApJS, 133, 321
Cayatte, V., van Gorkom, J. H., Balkowski, C., & Kotanyi, C. 1990, AJ, 100, 604
Dickey, J. M. 1997, AJ, 113, 1939
Doublier, V., Caulet, A., & Comte, G. 1999, A&AS, 138, 213
Duc, P.-A., & Mirabel, I. F. 1994, A&A, 289, 83
Duc, P.-A., & Mirabel, I. F. 1998, A&A, 333, 813
Duc, P.-A., Papaderos, P., Balkowski, C., et al. 1999, A&AS, 136, 539 (Paper I)
Duc, P.-A., Brinks, E., Springel, V., et al. 2000, AJ, 120, 1238
Duc, P.-A., Cayatte, V., Balkowski, C., et al. 2001a, A&A, 369, 763 (Paper II)
Duc, P.-A., Balkowski, C., Cayatte, V., et al. 2001b, Environmental Effects on H I-rich Dwarf Galaxies in the Hydra and Hercules Cluster, in Dwarf Galaxies and their Environment, ed. K. S. de Boer, R.-J. Dettmar, & U. Klein, 153
Duc, P.-A., & Amram, P. 2003, in preparation
Ferguson, H. C., & Binggeli, B. 1994, A&ARv, 6, 67
Fouqué, P., Bottinelli, L., Durand, N., Gouguenheim, L., & Paturel, G. 1990, A&AS, 86, 473
Freudling, W. 1995, A&AS, 112, 429
Fricke, K. J., Izotov, Y. I., Papaderos, P., Guseva, N. G., & Thuan, T. X. 2001, AJ, 121, 169
Gallagher, J. S., & Hunter, D. A. 1987, AJ, 94, 43
Giovanelli, R., Haynes, M. P., & Chincarini, G. L. 1981, ApJ, 247, 383
Goudfrooij, P., Hansen, L., Jorgensen, H. E., et al. 1994, A&AS, 104, 179
Guseva, N. G., Izotov, Y. I., Papaderos, P., et al. 2001, A&A, 378, 756
Hoffman, G. L., Helou, G., & Salpeter, E. E. 1988, ApJ, 324, 75

Heraudeau, P., & Simien, F. 1996, A&AS, 118, 111
Hopp, U., Kuhn, B., Thiele, U., et al. 1995, A&AS, 109, 537
Huang, Z., & Sarazin, C. L. 1996, ApJ, 461, 622
Huchra, J., Geller, M. J., Clemens, C. M., Tokarz, S. P., & Michel, A. 1995, The CfA Redshift Catalog (Cambridge: Harvard-Smithsonian Center for Astrophysics)
Kobulnicky, H. A., Kennicutt, R. C., & Pizagno, J. L. 1999, ApJ, 514, 544
Landolt, A. U. 1992, AJ, 104, 340
Makarova, L. 1999, A&AS, 139, 491
Matthews, L. D., van Driel, W., & Gallagher, J. S. 1998, AJ, 116, 1169
McGaugh, S. S. 1991, ApJ, 380, 140
McMahon, P. M. 1993, Ph.D. Thesis, Columbia University
Mirabel, I. F., & Wilson, A. S. 1984, ApJ, 277, 92
Papaderos, P., Loose, H.-H., Thuan, T. X., & Fricke, K. J. 1996, A&AS, 120, 207
Patterson, R. J., & Thuan, T. X. 1996, ApJS, 107, 103
Pilyugin, L. S. 2000, A&A, 362, 325
Pilyugin, L. S. 2001, A&A, 369, 594
Pilyugin, L. S., Mollá, M., Ferrini, F., & Vílchez, J. M. 2002, A&A, 383, 14
Rakos, K., Schombert, J., Maitzen, H. M., Prugovecki, S., & Odell, A. 2001, AJ, 121, 1974
Richer, M. G., & McCall, M. L. 1995, ApJ, 445, 642
Roberts, M. S., & Haynes, M. P. 1994, ARA&A, 32, 115
Rönnback, J., & Bergvall, N. 1994, A&AS, 108, 193
Salpeter, E. E., & Dickey, J. M. 1985, ApJ, 292, 426
Salzer, J. J., MacAlpine, G. M., & Boroson, T. A. 1989, ApJS, 70, 447
Sandage, A., & Brucato, R. 1979, AJ, 84, 472
Schommer, R. A., Sullivan III, W. T., & Bothun, G. D. 1981, AJ, 86, 943
Shields, G. A., Skillman, E. D., & Kennicutt, R. C. 1991, ApJ, 371, 82
Skillman, E. D., Bothun, G. D., Murray, M. A., & Warmels, R. H. 1987, A&A, 185, 61
Skillman, E. D., Kennicutt, R. C., Shields, G. A., & Zaritsky, D. 1996, ApJ, 462, 147
Tarenghi, M., Garilli, B., & Maccagni, D. 1994, AJ, 107, 1629
Thuan, T. X. 1985, ApJ, 299, 881
Valluri, M., & Jog, C. J. 1990, ApJ, 357, 367
van der Hulst, J. M. 1998, The Low Surface Brightness-Dwarf Galaxy Connection, in Dwarf Galaxies and Cosmology, ed. T. X. Thuân, C. Balkowski, V. Cayatte, & J. Trân Thanh Vân (Paris: Éditions Frontières), 313
van Driel, W., & van Woerden, H. 1989, A&A, 225, 317
van Driel, W., O'Neil, K., Cayatte, V., et al. 2003, A&A, 399, 433
van Zee, L., Salzer, J. J., Haynes, M. P., O'Donoghue, A. A., & Balonek, T. J. 1998, AJ, 116, 2805
van Zee, L. 2000, AJ, 119, 2757
van Zee, L. 2001, AJ, 121, 2003
Vennik, J., Hopp, U., & Popescu, C.C. 2000, A&AS, 142, 399
Vílchez, J. M. 1995, AJ, 110, 1090

# Online Material

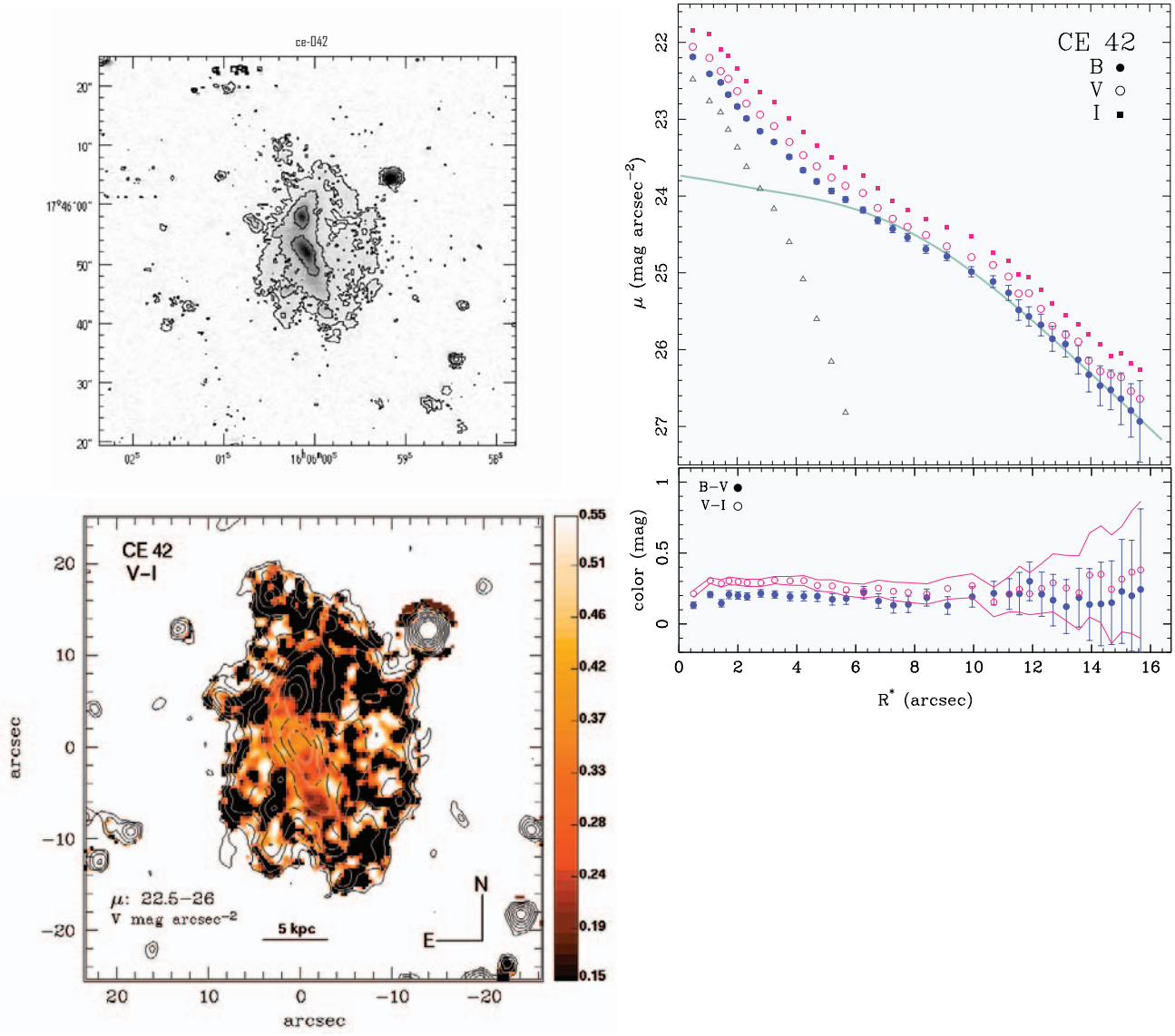


**Fig. 5.** Photometric properties of ce-042: **Upper left:** *V*-band image with superposed contours at 25.5, 24.5, 23.5, 22.5 and 21.5 mag arcsec$^{-2}$. The coordinates are in J2000.0 **Lower left:** ($V - I$) colour map with *V*-band contours superposed **Upper right:** Surface brightness profiles. The fitted surface brightness distribution of the LSB component in *B* is depicted by the thick/grey curve. Open triangles show the emission in excess of the LSB component **Lower right:** Colour profiles.

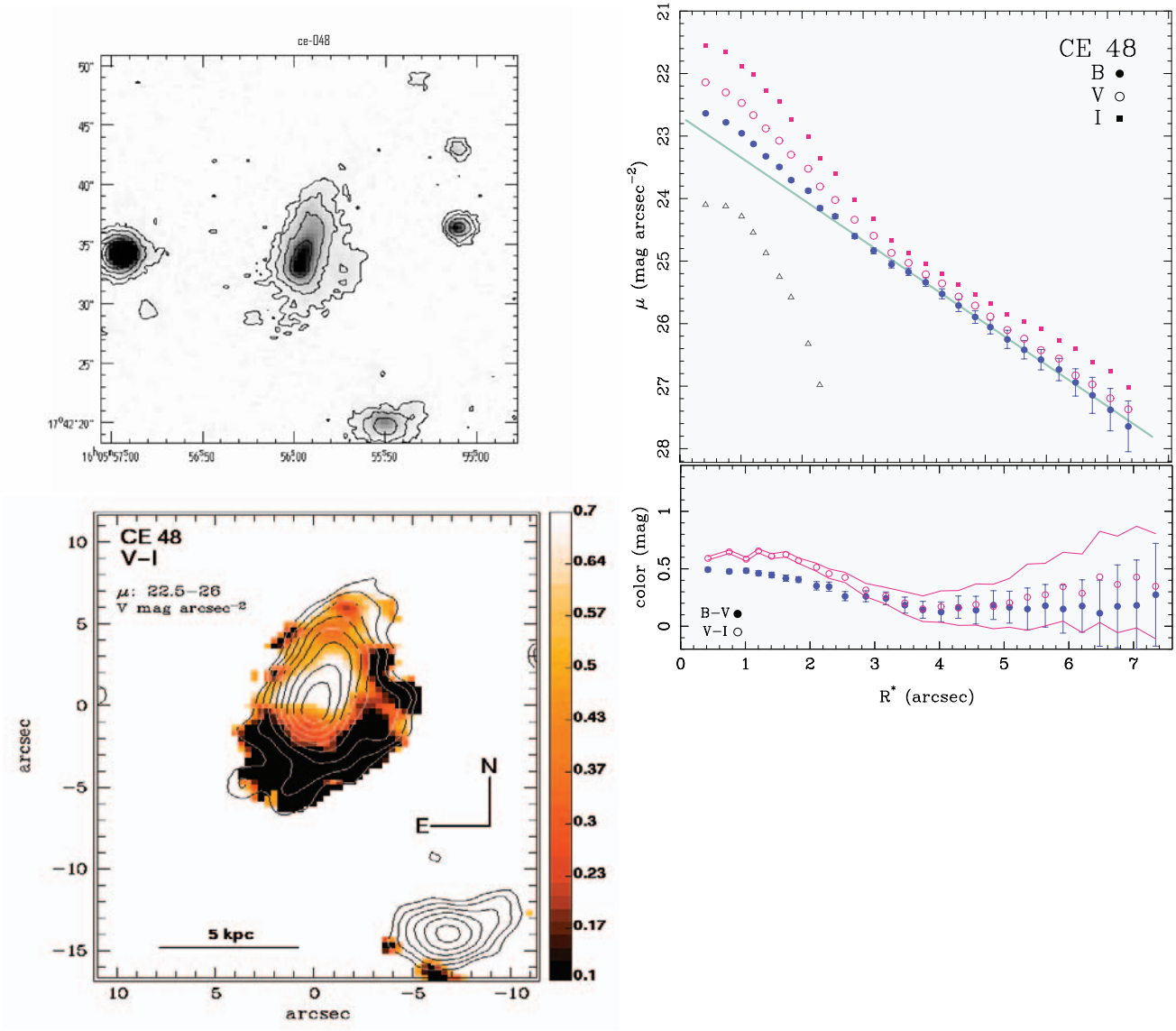


**Fig. 6.** Same as Fig. 5 for ce-048.

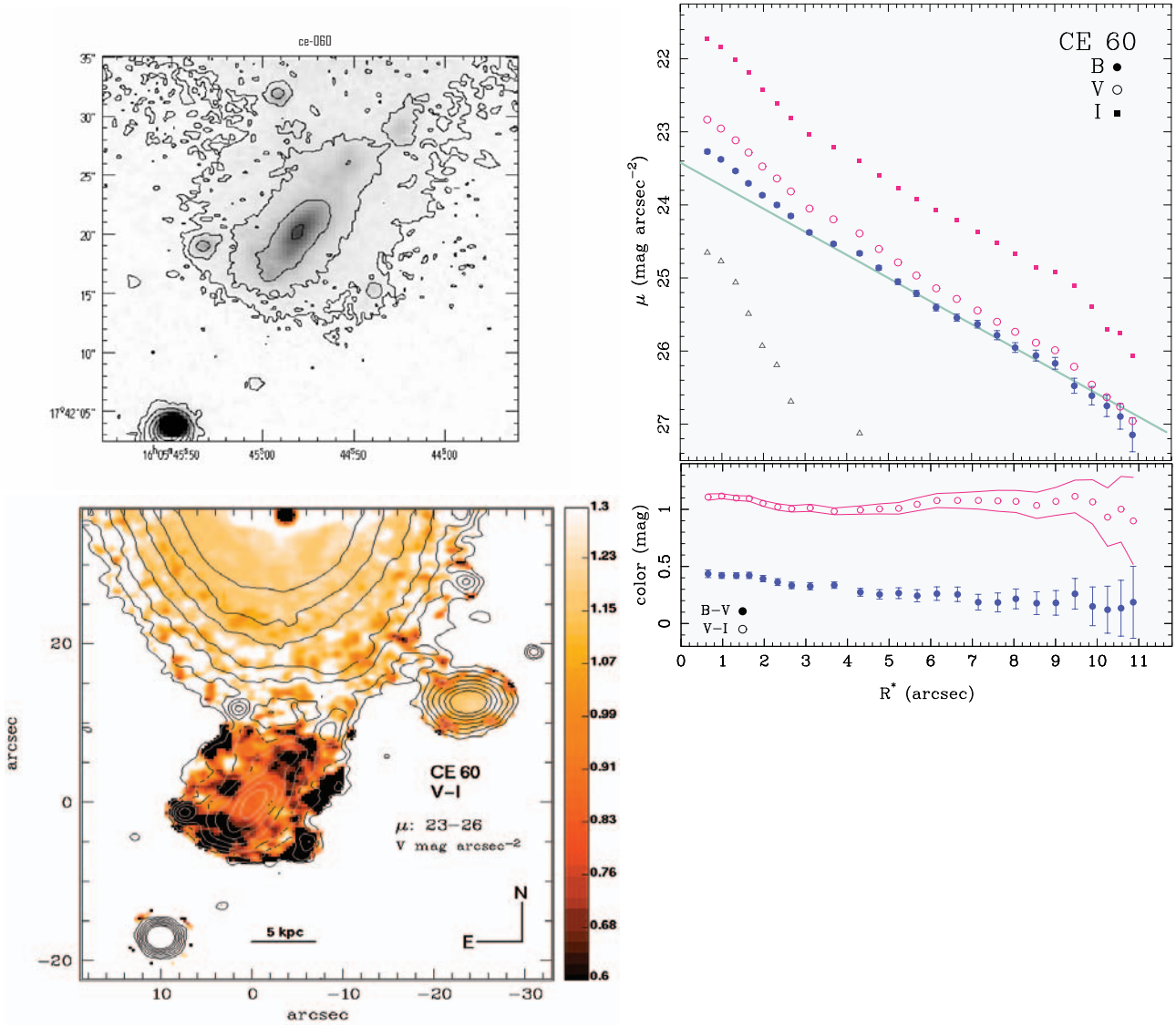


**Fig. 7.** Same as Fig. 5 for ce-060.

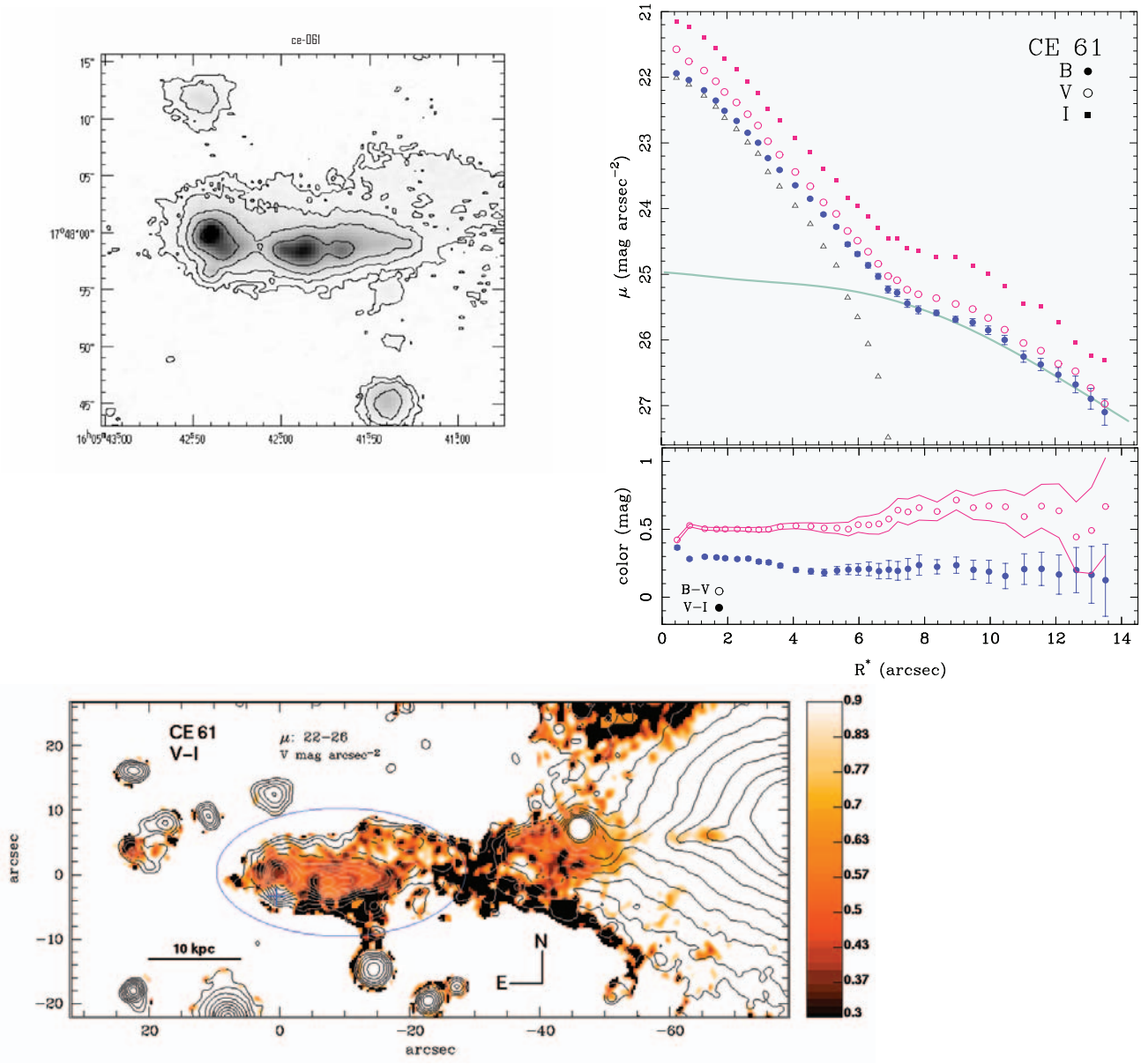


**Fig. 8.** Same as Fig. 5 for ce-061. The ellipse indicates the segment of tidal tail included in the surface photometry analysis. The small crosses in the maps show a red pointlike sources (probably a foreground star) which was removed before computing the SBPs.

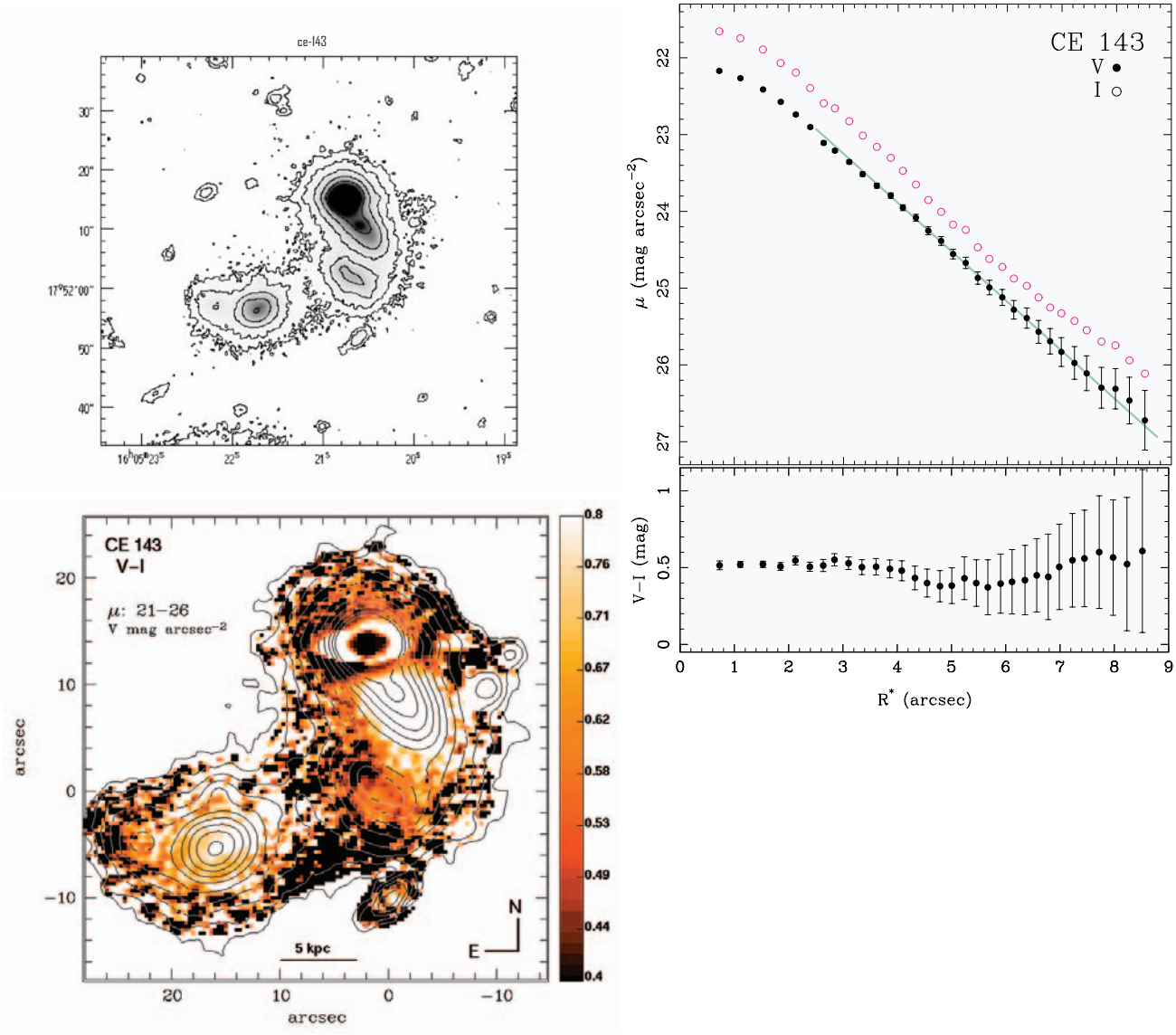


**Fig. 9.** Same as Fig. 5 for ce-143. Due to strong overlapping with nearby objects, a 2D model was fitted and subtracted from the original images in order to be able to disentangle the light of the H I-selected galaxy. Large uncertainties are expected in the SBP for $\mu_V > 25$ mag arcsec$^{-2}$.

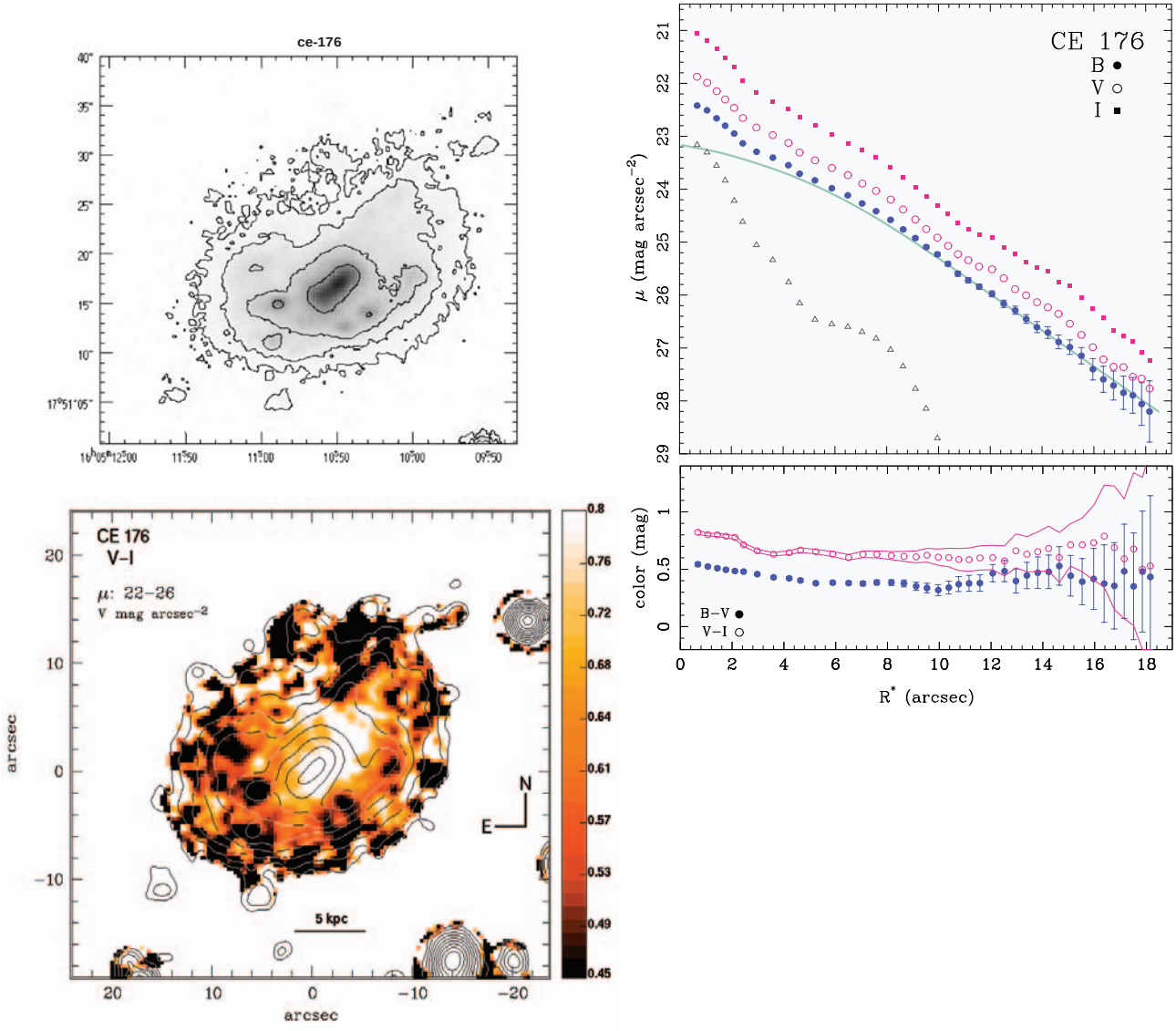


**Fig. 10.** Same as Fig. 5 for ce-176.

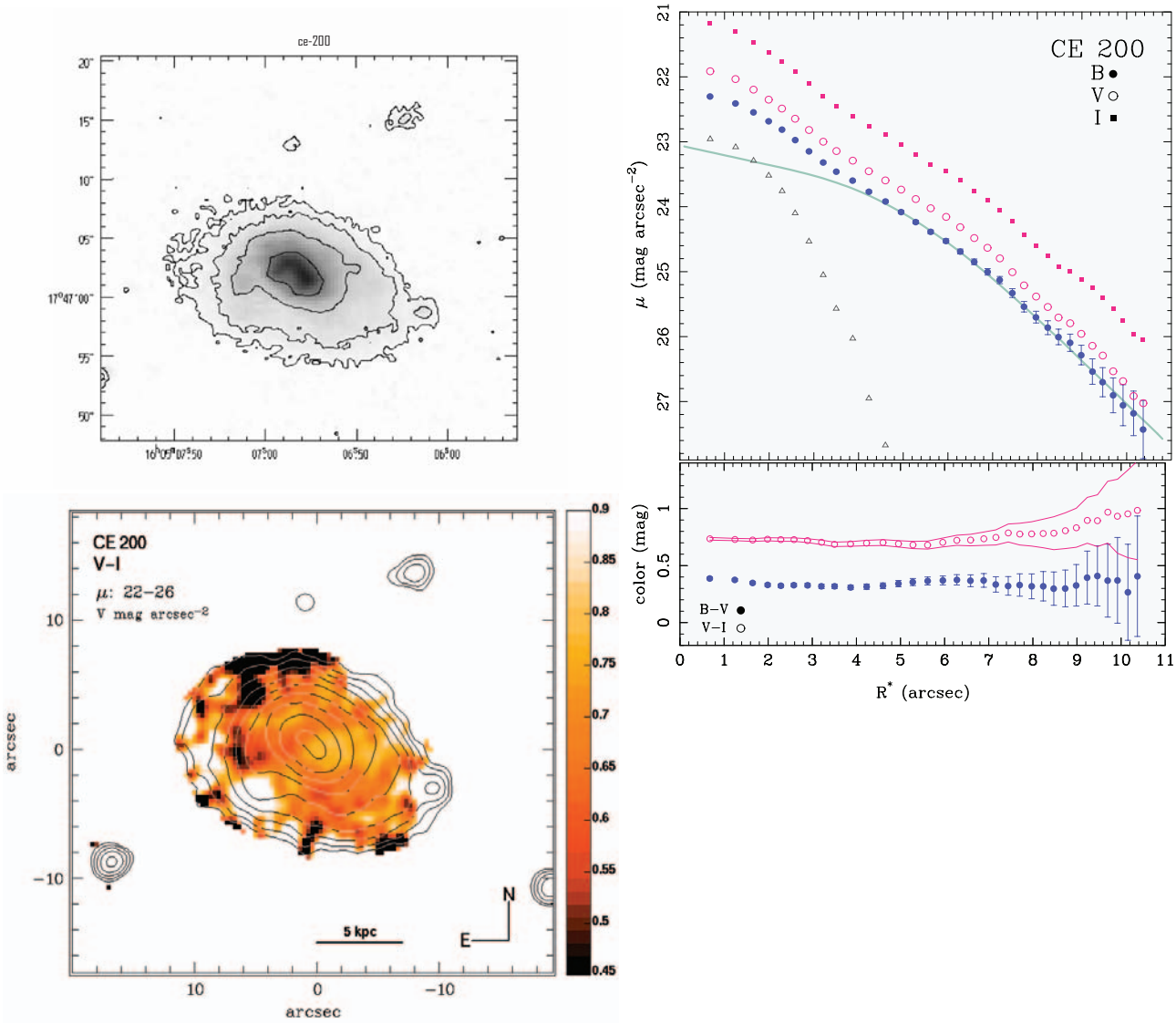


**Fig. 11.** Same as Fig. 5 for ce-200.

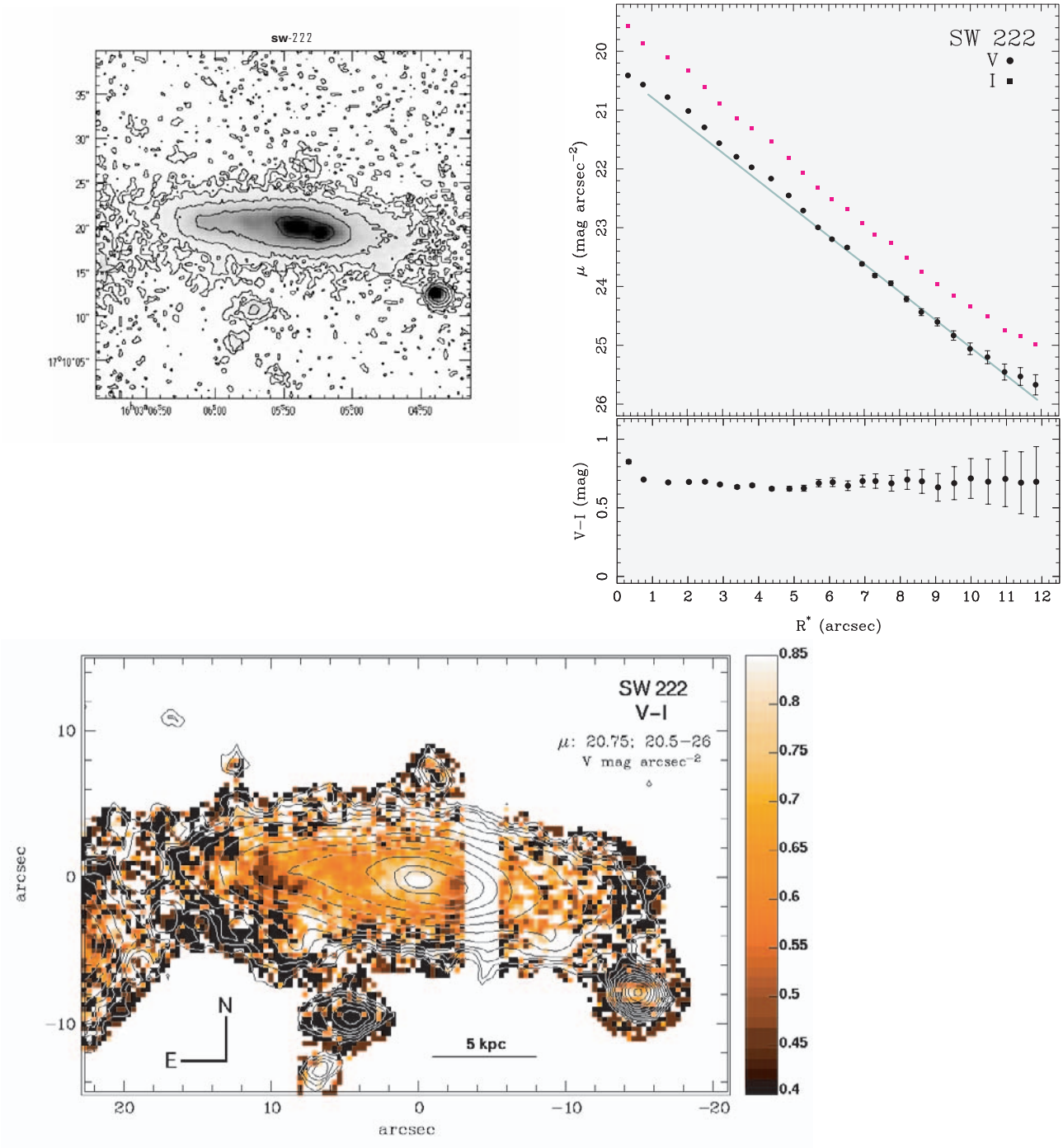


**Fig. 12.** Same as Fig. 5 for sw-222.

## Appendix A: Comments on individual objects

Included are comments regarding the H I properties, morphological appearance and environment of the sample galaxies.

*ne-112:* Although there is nearby galaxy detected in H I at a similar redshift, ne-176 at 5′.8 separation, no significant confusion is expected of the Arecibo H I spectrum. The D97 VLA data on ne-176 show $V_{\rm HI}$ = 11 101 km s$^{-1}$, $W_{50}$ = 508 km s$^{-1}$ and $I_{\rm ext}$ = 0.81 Jykm s$^{-1}$. In our spectrum its flux density contribution is expected to be at most a negligible ∼12% of the average flux density of ne-112.

*ne-178:* The uncertain optical redshift of 11 688 ± 251 km s$^{-1}$ listed in LEDA is based on two rather different measurements, 11 440 km s$^{-1}$ (Hopp et al. 1995) and 11 935 km s$^{-1}$ (Tarenghi et al. 1994). The VLA and Arecibo H I values of, respectively, 11 556 and 11 591 km s$^{-1}$ are rather closer to the former optical value. The VLA data show a clear velocity gradient from the SW to the NE.

*ne-204:* The VLA data show a highly extended H I distribution, but no mention is made of a velocity gradient in D97.

*ne-208:* The VLA detection is unresolved, with only 13 pixels above threshold, i.e. an area of about half a beam size.

*ne-240:* There are two nearby galaxies detected in H I with redshifts similar to that of ne-240, ne-250, at 3′.5 separation, and ne-208, at 5′.8 separation, which are expected to cause strong confusion with the profile of ne-240. Except for the 3.6 times higher $I_{\rm ext}$ line flux of ne-250, the VLA profile parameters of ne-240 and ne-250 are indistinguishable, seen the large velocity resolution, while ne-208 has a 90 km s$^{-1}$ lower velocity and 0.6 times the VLA flux of ne-240. At most, we expect the average flux density of nearby ne-250 and ne-208 in our spectrum to be, respectively, ∼125% and ∼30% that of ne-240.

*ne-250:* Its H I spectrum is not expected to be confused significantly by that of nearby ne-240 (see above), whose line emission is expected to be at most a negligible ∼11% of the average flux density of ne-250. The VLA data show an extended H I distribution with a clear velocity gradient from the NW to the SE.

*ne-398:* This reported VLA source was not confirmed by the Arecibo data. The VLA detection has a peak line flux density of 2.1 mJy in the integrated profile corresponding to the $I_{\rm H}$ integrated line flux (see Sect. 3.2), while the estimated mean flux density of the profile corresponding to the $I_{\rm ext}$ line flux is 4.1 mJy. Such a line should have been easily detectable with the 0.22 mJy noise level of our Arecibo data. However, instead of a strong, 352 km s$^{-1}$ wide profile centred on 10 602 km s$^{-1}$, at Arecibo we only marginally detected a 364 km s$^{-1}$ wide profile centred on 10 820 km s$^{-1}$, with a 3.2$\sigma$ peak after smoothing to a resolution of 19.5 km s$^{-1}$. Although the reported VLA source lies at the edge of the "ne" field, where the primary beam attenuation factor is 4, its detection seemed real, according to D97. Our Arecibo data indicate it was spurious.

*ce-042:* The published VLA profile parameters are uncertain as the detection lies just at the edge of the band. The VLA data show a velocity gradient from north to south. Our optical redshift of 11 840 ± 90 km s$^{-1}$ agrees within the uncertainties with the 11 959 ± 60 km s$^{-1}$ measured by Huchra et al. (1995). The colour gradient was found to be $\gamma_+ \approx 0$ mag kpc$^{-1}$ in both $B-V$ and $V-I$ for $R^* \geq 2''$. Mean $B-V$ and $V-I$ colours of 0.18 and 0.27 mag, respectively. The optical appearance of ce-042 is that of an Irregular galaxy. This object is almost isolated, with the elliptical galaxy PGC 057123 ($B_{\rm T}$ = 16.81) as its closest bright neighbour, at a distance of about 4′ and with a radial velocity difference of 1000 km s$^{-1}$.

*ce-048:* There are two nearby galaxies detected in H I with redshifts similar to that of ce-048, which are expected to cause confusion with its Arecibo profile: ce-060, at 2′.7 separation, and ce-095, at 6′.8 separation. There is only ±one VLA velocity channel (44 km s$^{-1}$) difference between their central H I velocities and that of ce-048; the VLA line widths of ce-048 and ce-060 are the same, 171 km s$^{-1}$, while that of ne-95 is twice as large. We expect the average flux density of nearby ce-060 and ce-095 in our spectrum to be, at most, respectively, ∼66% and ∼50% of that of ce-048. The VLA data show a quite extended distribution, with a velocity gradient from NW to SE. Its $\gamma_+ \approx= -0.05$ mag kpc$^{-1}$ in both colours, and its mean $B-V$ and $V-I$ colours are 0.27 and 0.38 mag, respectively. It appears as a faint blue galaxy, more compact than ce-042. There are several cluster galaxies near this object, the closest one being PGC 057115 ($B_{\rm T}$ = 16.84), a lenticular galaxy with 400 km s$^{-1}$ difference in radial velocity, 1′.1 away.

*ce-060*: Like in the case of ce-048 (see above), also for this pointing position serious confusion is expected at Arecibo between the H I lines of ce-048, ce-060 and ce-095. We expect the average flux density of nearby ce-048 and ce-095 in our spectrum to be, at most, respectively, ∼50% and ∼70% of that of ce-060. Its $\gamma_+ \approx= -0.04$ mag kpc$^{-1}$ in $B-V$ (mean colour 0.27 mag), and it shows practically no $V-I$ colour gradient, with a mean $V-I$ colour of 1.04 mag. In its vicinity lies the bright Sab galaxy IC 1185 ($B_{\rm T}$ = 14.89), at a distance of 0′.7, with a velocity difference between both galaxies of about 700 km s$^{-1}$.

*ce-061*: An extended H I distribution, measuring at least 2′.3 in the E-W direction, surrounds the peculiar galaxy IC 1182 ($B_{\rm T}$ = 15.37, $V_{\rm opt}$ = 10 223 km s$^{-1}$), formed to the East by the VLA source ce-061 and to the West by the much weaker source ce-086. In the optical, IC 1182 shows a jet-like structure towards the East, following the direction of the H I distribution. The target galaxy ce-061 lies at the tip of the H I tail extending eastwards from IC 1182, at about 1′.5 from the centre of IC 1182. The CCD image of ce-061 (Fig. 8) shows two distinct peaks, and the maximum in the H I tail coincides, within the 25″ beam size, with the easternmost optical peak. The SBP has been taking over the area covering both concentrations seen in Fig. 8. A recent H$\alpha$ line Fabry-Pérot velocity field (Duc & Amram 2003) shows that ce-061 is a gravitationally bound system inside the tidal tail of the IC 1182 merger system, confirming its interpretation as a tidal dwarf galaxy by Braine et al. (2001), who detected about $7 \times 10^9$ $M_\odot$ of $H_2$ in a resolved distribution in IC 1182, but failed to detect ce-061 in the CO(1-0) or (2-1) lines, putting an upper limit to its $H_2$ mass of about $6 \times 10^7$ $M_\odot$. We obtained Arecibo H I spectra of ce-061 and ce-086, with pointing centres corresponding to the VLA H I positions, which are 1′.8 (half the Arecibo HPBW) apart. Though the two peaks that can be identified

with the VLA profiles of ce-061 and ce-086 are clearly present in our spectrum, centered on ∼10 080 and 10 450 km s$^{-1}$, respectively, the latter component is much stronger than in the VLA profiles: the average flux density in both components is about 16 and 2 mJy at the VLA, using the $I_{\rm ext}$ fluxes, while their peak fluxes are ∼15 and 6 mJy in the Arecibo profile centered on ce-061 and ∼9 and 6 mJy in the profile centered on ce-086. This may be due to extended emission in the distribution not included in the VLA profiles. The VLA data show a fairly smooth velocity gradient along the major axis of the H I distribution and very little gas between the two peaks, at 10 200–13 000 km s$^{-1}$, in the area of IC 1182 itself. $\gamma_+ \approx= -0.013$ mag kpc$^{-1}$ in $B-V$ (mean colour 0.22 mag); $V-I$ colour gradient of 0.016 mag kpc$^{-1}$, mean colour 0.56 mag. H I detections of IC 1882 were also reported by Bieging & Biermann (1983), Bird et al. (1993), Bothun et al. (1981, 1985), Mirabel & Wilson (1984), Salpeter & Dickey (1985) and Schommer et al. (1981). The average profile parameters from these references are $V_{\rm HI} = 10\,239 \pm 62$ km s$^{-1}$, $W_{20} = 592 \pm 48$ km s$^{-1}$ and $I_{\rm HI} = 3.6 \pm 0.8$ Jy km s$^{-1}$. These values correspond well with our Arecibo parameters for ce-61 of 10 263 km s$^{-1}$, 666 km s$^{-1}$ and 3.4 Jy km s$^{-1}$, respectively.

*ce-143*: The CDD images show three, overlapping object. The peak of the VLA H I distribution corresponds to the object in the middle, the weakest of the three. Before determining its morphological component, two-dimensional model light distributions of its two neighbours were subtracted from the images. Zero colour gradient, mean $V - I$ colour of 0.48 mag. The optical counterpart of this galaxy seems to be a triple nucleated source, with the H I cloud centred on the middle one. At a distance of 0.′7 of this system we find the Sa galaxy PGC 057055, with $B_{\rm T} = 15.88$, which shows a radial velocity more than 700 km s$^{-1}$ higher than ce-143.

*ce-176*: Although the VLA data show a galaxy in the vicinity with a similar redshift, ce-200, we do not expect our Arecibo profile to be confused with it: at 4.′4 distance, it has only a 22 km s$^{-1}$ higher central velocity than ce-176, but its mean VLA line flux is three times smaller. We expect the average flux density of ce-200 in our spectrum to be, at most, a negligible 7% of that of ce-176. The VLA data show a very extended H I distribution. The galaxy shows practically a zero gradient in both colour profiles, and mean $B - V$ and $V - I$ indices of 0.42 mag and 0.66 mag, respectively. This galaxy appears like a dwarf Irregular galaxy with a very extended H I disc. Also, some knots of star formation are seen in the optical images. The closest bright companion of this galaxy, at a distance of 2.′5, is PGC 057020 ($B_{\rm T} = 16.22$), an SB0/Sa galaxy with a radial velocity difference of about 1000 km s$^{-1}$ with respect to ce-176.

*ce-200*: The Arecibo spectrum of this object shows three peaks: one around 9780 km s$^{-1}$ another around 9940 km s$^{-1}$ and an about 300 km s$^{-1}$wide feature around ∼10 200 km s$^{-1}$. Though the centre peak is very close in velocity to ce-200, it is expected to be seriously confused with emission from nearby ce-176 (see above). We expect the average flux density of ce-176 in our spectrum to be, at most, equal to that of ce-200. No object can be found in the VLA data that might cause the peak at 9780 km s$^{-1}$, while the third peak appears due to ce-199, at 1.′6 distance, for which the VLA data show a $V_{\rm HI}$ of 10 204 km s$^{-1}$, a FWHM of 284 km s$^{-1}$and a mean flux density of 1.5 mJy. $\gamma_+ \approx 0$ mag kpc$^{-1}$ in $B - V$; mean colour 0.34 mag. The $V - I$ profile shows a slight colour gradient of ≈0.03 mag kpc$^{-1}$ and a mean value of 0.77 mag. No morphological peculiarities are apparent for this galaxy. Although it shows no signs of tidal interaction, two bright galaxies appear close to it, showing also a similar radial velocity: NGC 6043A ($V = 9879$ km s$^{-1}$ and $B_{\rm T} = 14.10$) and NGC 6045 ($V = 9986$ km s$^{-1}$ and $B_{\rm T} = 14.87$), classified, respectively, as S0 and Sc, and located at distances of 1.′3 and 1.′6 from ce-200.

*sw-103*: the VLA data show a velocity gradient from northeast to southwest. See also Sects. 3.2.4 and 4.

*sw-194:* The strong (713 mJy), extended continuum source in the nearby galaxy NGC 6034 made sensitive Arecibo line observations impossible and the VLA detection tentative. The VLA profile is weak (0.75 mJy peak in the $I_{\rm H}$ profile) and there are only 15 pixels above the detection threshold. The "line" could be a figment of imperfect bandpass calibration and continuum subtraction, as the continuum is sufficiently strong to increase the noise in the spectral baselines in its vicinity (D97). See also Sects. 3.2.4 and 4.

*sw-222*: The VLA data show an extended H I distribution, with a plume extending about 1′ towards the SE from the centre, and a velocity gradient along the main body from west to east. $\gamma_+ \approx 0$ mag kpc$^{-1}$ in $V - I$; mean colour 0.68 mag. This galaxy shows an elongated shape with an H I plume extending towards the South. The closest bright galaxy, which is located 4 arcmin away, is the lenticular PGC 056824 ($B_{\rm T} = 14.00$), whose velocity difference with sw-222 is about 300 km s$^{-1}$.

*47-138* No sensitive Arecibo observations could be obtained due to the presence of the 1.2 Jy radio source 4C+15.53, whose centre is just 40″ offset from the galaxy. It could be detected at the VLA as the continuum source has a diameter of about 100″ and the VLA peak flux density, 50 mJy/beam, is low enough not to disturb the H I detection (1.1 mJy peak in the $I_{\rm H}$ profile). The VLA data show a velocity gradient from north to south.

*47-154* This weak VLA source was not detected at Arecibo. The VLA detection has a peak line flux of 0.7 mJy in the integrated profile corresponding to the $I_{\rm H}$ integrated line flux (see Sect. 3.1), while the estimated mean flux density of the profile corresponding to the $I_{\rm ext}$ line flux is 0.37 mJy. It is classified as a somewhat tentative detection in D97. With an 0.32 mJy rms noise level in our Arecibo data, this source appears too weak for detection or confirmation.

*47-211* The VLA data show a velocity gradient from NE to SW, along the major axis of the galaxy.